EVALUATION OF THE ROLE OF EXCITOTOXICITY IN AN EXPERIMENTAL MODEL OF RABIES IN MICE

by

Courtney Anne Scott

A thesis submitted to the Centre for Neuroscience Studies

in conformity with the requirements for

the degree of Master of Science

Queen's University

Kingston, Ontario, Canada

July, 2007

Copyright © Courtney Anne Scott, 2007

Library and Archives Canada

Published Heritage Branch

395 Wellington Street
Ottawa ON K1A 0N4
Canada

Bibliothèque et Archives Canada

Direction du Patrimoine de l'édition

395, rue Wellington
Ottawa ON K1A 0N4
Canada

Your file Votre référence
ISBN: 978-0-494-30245-3
Our file Notre référence
ISBN: 978-0-494-30245-3

NOTICE:
The author has granted a non-exclusive license allowing Library and Archives Canada to reproduce, publish, archive, preserve, conserve, communicate to the public by telecommunication or on the Internet, loan, distribute and sell theses worldwide, for commercial or non-commercial purposes, in microform, paper, electronic and/or any other formats.

The author retains copyright ownership and moral rights in this thesis. Neither the thesis nor substantial extracts from it may be printed or otherwise reproduced without the author's permission.

AVIS:
L'auteur a accordé une licence non exclusive permettant à la Bibliothèque et Archives Canada de reproduire, publier, archiver, sauvegarder, conserver, transmettre au public par télécommunication ou par l'Internet, prêter, distribuer et vendre des thèses partout dans le monde, à des fins commerciales ou autres, sur support microforme, papier, électronique et/ou autres formats.

L'auteur conserve la propriété du droit d'auteur et des droits moraux qui protège cette thèse. Ni la thèse ni des extraits substantiels de celle-ci ne doivent être imprimés ou autrement reproduits sans son autorisation.

In compliance with the Canadian Privacy Act some supporting forms may have been removed from this thesis.

While these forms may be included in the document page count, their removal does not represent any loss of content from the thesis.

Conformément à la loi canadienne sur la protection de la vie privée, quelques formulaires secondaires ont été enlevés de cette thèse.

Bien que ces formulaires aient inclus dans la pagination, il n'y aura aucun contenu manquant.

Canada

ABSTRACT

Rabies is one of the most lethal of all infectious diseases. It is thought that the severe clinical illness and fatal outcome is due to neuronal dysfunction, rather than neuronal death, because only mild histopathological lesions are found under natural conditions. In this study, we examine the hypothesis that excitotoxicity may serve as a basis for neuronal dysfunction in rabies virus infection.

The administration of ketamine (60mg/kg intraperitoneally q12h) to adult ICR mice inoculated intracerebrally or in the hindlimb footpad with the challenge virus standard (CVS-11) strain of rabies virus did not result in reduced mortality or the amelioration of clinical neurological disease compared to the administration of vehicle. Therapy with ketamine did not reduce the number of infected neurons in various brain regions or the severity of apoptotic changes in the brains of intracerebrally-inoculated mice.

Transgenic mice expressing yellow fluorescent protein (YFP) in neurons and inoculated in the hindlimb footpad with CVS displayed beading and fragmentation of the dendrites and axons of layer V pyramidal neurons in the cerebral cortex, cerebellar mossy fibers and axon tracts in the brainstem, whereas neuronal processes in the hippocampus and perikarya showed relatively few changes under fluorescent microscopy. These morphological abnormalities differ from the beading observed in excitotoxicity, which is particularly severe in the hippocampus and is characterized by selective dendritic injury.

Toluidine blue staining of plastic embedded tissues revealed vacuoles within the perikarya and proximal dendrites of pyramidal neurons in the cerebral cortex and hippocampus of YFP mice, and larger vacuolation within the neuropil of the cerebral cortex. Ultrastructurally, the neuropil vacuolation primarily represented swollen neuronal

processes and pre-synaptic nerve endings, while the cytoplasmic vacuoles corresponded with swollen mitochondria. Mitochondrial swelling is a typical feature of excitotoxic injury, but excitotoxicity is also associated with microtubule fragmentation, which was not observed in the present study. Overall, we feel that the evidence does not support an important role for excitotoxicity in experimental rabies. Furthermore, the structural abnormalities observed in YFP mice support a role for severe neuronal injury without prominent neuronal death in rabies virus infection, as opposed to neuronal dysfunction without morphological changes.

ACKNOWLEDGEMENTS

Firstly, I would like to thank my supervisor, Dr. Jackson, for the opportunity to expand my research skills and for the guidance along the way. I have gained much, both academically and personally, from this experience. I would also like to thank Dr. Rossiter for his support and help with histopathological and ultrastructural analysis, Dr. Weli for his encouragement and input, Dr. Andrew for his transgenic mice and use of his laboratory equipment, John DaCosta for his assistance with electron microscopy and Gail Lawrance for her vast knowledge of staining protocols.

Thank you to my lab mates in the Jackson and Andrew labs, especially Lee, Heather, James, Gaby, Elizabeth and Becca. This experience would not have been the same without you.

Lastly, I would like to thank my parents and brother, Cameron, for their everlasting support. I know it has been trying at times, but I could not have finished this degree without you.

TABLE OF CONTENTS

LIST OF TABLES

LIST OF FIGURES

LIST OF ABBREVIATIONS

5-HT	serotonin
ACh	acetylcholine
AG	aminoguanidine
AIF	apoptosis-inducing factor
AMPA	α-amino-3-hydroxy-5-methly-4-isoxazole propionate
B_{max}	maximum binding
CJD	Creutzfeldt-Jakob disease
CNS	central nervous system
CVS	challenge virus standard
DAB	3,3-diaminobenzidine tetrachloride
dH_2O	distilled water
DNA	deoxyribonucleic acid
EEG	electroencephalographic
G	glycoprotein
HE	hematoxylin-eosin
IEG	immediate-early-response gene
iNOS	inducible nitric oxide synthase
kainite	kainic acid
L	RNA-dependent RNA polymerase
LC8	dynein light chain
M	matrix protein
MAP-2	microtubule-associated protein 2
MTP	mitochondrial permeability transition pore
N	nucleoprotein
NGS	normal goat serum
NMDA	N-methyl-D-aspartate
NO	nitric oxide
P	phosphoprotein
PBS	phosphate buffered saline
pENK	proenkephalin
p.i.	post-inoculation
QNB	quinuclidinyl benzylate
REM	rapid eye movement
RNA	ribonucleic acid
ROS	reactive oxygen species
RSA	rhythmic slow activity
TdT	terminal transferase
TME	transmissible mink encephalopathy
TSE	transmissible spongiform encephalopathie
TUNEL	transferase-mediated dUTP nick-end labelling
YFP	yellow fluorescent protein

CHAPTER 1: INTRODUCTION

I. The Rabies Virus

The rabies virus is a highly neurotropic virus which causes acute infection of the central nervous system (CNS) for which there is no effective antiviral therapy in humans. The rabies virus belongs to the *Lyssavirus* genus within the *Rhabdoviridae* family. Rabies virions are rod- or bullet-shaped particles measuring 180nm in length and 75nm in diameter (Wunner, 2007). The single-stranded negative-sense RNA genome of the rabies virus encodes five proteins: nucleoprotein (N), phosphoprotein (P), matrix protein (M), glycoprotein (G) and RNA-dependent RNA polymerase (L) (Wunner, 2007). The G protein makes up the surface projections of the virus, which contain the cell surface receptors and antibody binding sites, and is essential for pathogenicity (Wunner, 2007).

II. Epidemiology of Rabies Virus Infection

Rabies is thought to be the most lethal of all infectious diseases. It is estimated that there are 55,000 deaths per year largely due to endemic canine rabies in developing countries of Asia and Africa (WHO, 2005). In Canada and the United States, most human cases of rabies involve bats, while other common vectors include raccoons, skunks and foxes (Jackson, 2000; Jackson, 2006). In 2004, there were seven iatrogenic cases of rabies in Texas and Germany following organ transplantations from patients with undiagnosed rabies (Hellenbrand *et al.*, 2005; Srinivasan *et al.*, 2005). Also in 2004, a patient in Wisconsin was the first to survive rabies without administration of the rabies vaccine prior to the onset of clinical disease (Willoughby *et al.*, 2005). Oral vaccination of wildlife with live attenuated rabies virus or recombinant rabies virus vaccines is the most effective method to control rabies and may lead to the eradication of this lethal disease

(CDC, 1999). Although human rabies encephalitis remains untreatable in nearly all cases, the infection is preventable.

III. Rabies Pathogenesis

Rabies virus is transmitted in the saliva of mammals. Entry of the virus occurs in subcutaneous tissues or muscle as the result of wounds or through direct contact with mucosal surfaces (Jackson, 2000). During the incubation period in natural rabies, which typically lasts from weeks to months, the virus remains close to the site of inoculation (Charlton *et al*, 1997; Jackson, 2006). It has been hypothesized that viral replication in muscle fibers during the incubation period may be necessary to generate sufficient amounts of virus for entry into the peripheral nervous system (Charlton and Casey, 1981). However, other studies have shown that the virus can enter nerve terminals directly without replication in muscle, particularly in experimental models using fixed rabies virus strains (Shankar *et al.*, 1991; Lewis *et al.*, 2000).

The co-localization of rabies virus antigen and α-bungarotoxin, which identifies neuromuscular junctions, suggests a high concentration of rabies virus receptors at this site (Lewis *et al.*, 2000). Furthermore, α-bungarotoxin and d-tubocurarin, ligands of the nicotinic acetylcholine receptor, prevent the infection of cultured myotubes and peripheral nerve fibers, indicating that the nicotinic acetylcholine receptor may serve as a peripheral receptor for the virus (Lentz *et al.*, 1982). However, the distribution of the virus is not restricted to the cholinergic system (Reagan and Wunner, 1985). Other putative receptors include the neural cell adhesion molecule (Thoulouse *et al.*, 1998) and the p75 neurotropin receptor (Tuffereau *et al.*, 1998; Langevin *et al.*, 2002). The neural cell adhesion molecule is also expressed in adult muscle and at the neuromuscular

junction (Moscoso *et al.*, 1998; Polo-Parada *et al.*, 2001).

Once the virus gains entry into peripheral nerve terminals via receptor mediated endocytosis or membrane fusion, it then travels towards the CNS (centripetal spread) within motor and sensory axons at a rate of approximately 50-100 mm per day (Tsiang *et al.*, 1991a; Gaudin *et al.*, 1999). Transection of nerve fibers (Baer and Lentz, 1991) or disruption of axoplasmic transport by colchicine (Tsiang, 1979), a microtubule-disrupting agent, reduce mortality in animals and indicate that the centripetal spread of the virus is mediated by fast axoplasmic transport. Furthermore, the use of the rabies virus as a neuroanatomical tracer to define circuits of synaptically linked neurons in rodents and primates has shown that axonal transport of the rabies virus occurs exclusively in the retrograde direction (Tang *et al.*, 1999; Kelly and Strick, 2000). Evidence has also shown that the rabies virus phosphoprotein interacts with the cytoplasmic dynein light chain (LC8), which is important in actin-based vesicle transport and microtubule-directed organelle transport in axons (Jacob *et al.*, 2000; Raux *et al.*, 2000). However, the role of this interaction in the axonal transport of the ribonucleocapsid complex has yet to be confirmed.

Once the virus reaches the spinal cord there is rapid and widespread dissemination throughout the CNS. This occurs via direct transneuronal transfer of virus from perikarya and dendrites to adjacent axon terminals due to viral budding (Charlton and Casey, 1979) and intra-axonal spread along neuroanatomical pathways (Ceccaldi *et al.*, 1989). In mice infected with the challenge virus standard (CVS) strain of fixed rabies virus, the pattern of infection in the pyramidal neurons of the hippocampus while sparing of the granule cells in the dentate gyrus has raised speculation that infection may be dependent on the presence of N-methyl-D-aspartate (NMDA) NR1 receptors (Gosztonyi and Ludwig,

2001). This is because (1) rabies virus spreads exclusively by retrograde fast axonal transport and, therefore, cannot infect granule cells by the perforant path and (2) mossy fibers from CA3 predominantly have α-amino-3-hydroxy-5-methly-4-isoxazole propionate (AMPA) and kainate receptors, not NMDA receptors.

Replication of the rabies virus in the CNS is followed by its spread away from the CNS (centrifugal spread) along neuronal pathways, particularly involving the parasympathetic nervous system, back to peripheral tissues. At this late stage, intact viral particles can be found in the peripheral nerve axons, unlike the exclusive presence of bare nucleocapsids found during the centripetal phase of viral migration (Gosztonyi *et al.*, 1993). This final step in the dissemination of the virus is responsible for the infection of the salivary glands, skeletal and cardiac muscle, adrenal glands, kidneys, retina, cornea, pancreas and nerves around hair follicles (Jackson *et al.*, 1999). In rabies vectors, viral replication and budding from plasma membranes in the periphery takes place predominantly in the salivary glands, releasing virus that is transmissible to other mammals (Warrell and Warrell, 2004).

IV. Rabies Pathology

A. Encephalomyelitis

The characteristic pathological feature of rabies virus infection of humans and animals is acute encephalomyelitis, which is a neurological disorder characterized by inflammation of the brain and spinal cord. Inflammatory infiltrates, including lymphocytes and monocytes and a small number of plasma cells, are found in the leptomeninges and parenchyma (Tangchai *et al.*, 1970; Rossiter and Jackson, 2007). Additionally, perivascular cuffing with mononuclear cells and microglial nodules known

as Babes nodules are observed in the brainstem and spinal cord (Rossiter and Jackson, 2007). Although these inflammatory features are observed in a majority of rabies cases, they are not unique to rabies. Babes nodules, which are microscopic accumulations of activated microglia surrounding chromatolytic and degenerating neurons, are also seen in other viral encephalitis and infectious disorders (Babes, 1892; Love and Wiley, 2002). Also, Iwasaki *et al.* (1993) reported a fatal rabies case with virtually no inflammation or tissue injury. Thus, fatal encephalitic rabies is not always associated with significant inflammation.

One feature that is unique to rabies virus infection is the presence of Negri bodies. Negri bodies are round or oval shaped eosinophilic inclusions that are found in the cytoplasm of infected neurons (Rossiter and Jackson, 2007). They consist of viral particles embedded in an amorphous or slightly electron-dense matrix containing randomly oriented viral nucleocapsids (Gonzalez-Angulo *et al.*, 1970). There is also a small, basophilic/granular inner body within Negri body inclusions which differentiate this type of inclusion from one found in healthy neurons known as lyssa bodies (Negri, 1903; Negri, 1909). Within an individual neuron, Negri bodies may be single or multiple and are typically located in the perikaryon, but may occasionally be found in dendrites and axons. Although Negri bodies are a specific diagnostic lesion in rabies infection, this is only true in 50-90% of natural infections with the wild or "street" rabies virus strain. They are almost never observed in infection with "fixed" rabies virus strains, which are strains passaged in the laboratory (Kristensson *et al.*, 1996). As such, their pathogenic significance remains unclear.

B. Apoptosis

Apoptosis, or programmed cell death, is an important cellular response that allows organisms to eliminate cells that have been produced in excess, developed improperly or sustained damage in order to maintain homeostasis (Thompson, 1995). It is also a common mechanism by which viruses cause injury to host cells (Razvi and Welsh, 1995). Apoptosis is orchestrated by genetic programs that signal the cell to utilize its own energy to synthesize macromolecules which results in its own demise. There are two major apoptotic pathways: caspase-dependent and caspase-independent. Both induce characteristic morphological features which include oligonucleosomal DNA fragmentation, multiple condensations of nuclear chromatin, plasma membrane bleb formation, cell shrinkage and budding off of cellular fragments (apoptotic bodies), while cytoplasmic membranes and organelle integrity are preserved (Bredesen, 1995).

The caspase-dependent pathway plays a vital role in the induction, transduction and amplification of intracellular apoptotic signals (Fan *et al.*, 2005). Caspases are aspartate-specific cysteine proteases which are present in the cell in an inactive form and are irreversibly activated during apoptosis, leading to changes in ultrastructure, chromatin condensation and nuclear fragmentation (Thoulouze *et al.*, 2003). Alternative pathways that do not utilize caspases involve noncaspase proteases such as cathepsins or calpain (Leist and Jaattela, 2001) or the mitochondrial apoptosis-inducing factor (AIF) (Daugas *et al.*, 2000). AIF is a flavoprotein oxidoreductase which is found in the mitochondrial intermembrane space. When cells initiate apoptosis AIF is released into the cytosol and is then translocated to the nucleus where it induces chromatin condensation and DNA fragmentation (Thoulouze *et al.*, 2003).

Apoptosis can be blocked by the expression of anti-apoptotic genes such as the

Bcl-2 proto-oncogenes. Bcl-2 is a protein that is located on the cytoplasmic surface of the mitochondrial outer membrane, the endoplasmic reticulum membranes and on the nuclear envelope (Thoulouze *et al.*, 2003). It serves to stabilize the mitochondrial membrane functions in a number of ways. Firstly, Bcl-2 controls the release of cytochrome *c*, an intermediate in apoptosis, by preventing the activation of the caspase pathway and the caspase-induced degradation of intracellular proteins (Yang *et al.*, 1997). Bcl-2 also exhibits antioxidative properties which inhibit the production of reactive oxygen species (Reed, 1998). AIF translocation to the nuclease is also inhibited by Bcl-2 overexpression (Susin *et al.*, 1996).

Apoptosis has been found to play an important role in the pathogenesis of rabies virus infection, but only under certain experimental conditions. In suckling and adult mice inoculated intracerebrally with the CVS strain of fixed rabies virus, widespread apoptosis was observed in the cerebral cortex and hippocampus (Jackson and Rossiter, 1997; Jackson and Park, 1998). CVS also induces apoptosis in rat prostatic adenocarcinoma (AT3) cells (Jackson and Rossiter, 1997), mouse neuroblastoma cells (Theerasurakarn and Ubol, 1998) and mouse embryonic hippocampal neurons (Morimoto *et al.*, 1999), while Purkinje cells of the mouse and rat embryonic spinal motor neurons are more resistant to apoptotic cell death (Guigoni and Coulon, 2002). This finding suggests that the mechanism of induction of cell death may be different between various neuronal cell types. Furthermore, there is an age dependent susceptibility to apoptosis with suckling mice demonstrating more apoptosis in more neuronal cell types than adult mice inoculated intracerebrally with CVS (Jackson and Park, 1998).

In natural rabies, the role of apoptosis is even less clear. Morphological observations indicate that neuronal apoptosis does not play a prominent role in human

rabies (Fu and Jackson, 2005; Juntrakul *et al.*, 2005). Adle-Biassette and colleagues (1996) describe a unique rabies case in which foci of deoxynucleotidyl transferase-mediated dUTP nick-end labelling (TUNEL)-positive neurons were observed in the brainstem and hippocampus. However, the presence of morphological features of apoptosis is very important. Apoptosis is also not seen in experimental infection of peripherally inoculated animals, which more closely reflects natural rabies than intracerebral inoculation (Reid and Jackson, 2001).

Apoptosis may be a protective rather than pathogenic mechanism in rabies virus infection because less pathogenic viruses induce more apoptosis than more pathogenic viruses both *in vitro* (Morimoto *et al.*, 1999) and *in vivo* (Jackson *et al.*, 2006) using peripheral routes of inoculation. The destruction of rabies virus infected cells by apoptosis may serve to restrict viral propagation during infection and thus limit neuroinvasion and transmission to other animals. This is supported by the finding that minocycline, a tetracycline-derivative with anti-apoptotic properties, exacerbates clinical disease and results in more infected neurons in the hippocampus of suckling mice infected with CVS via the hindlimb thigh muscle (Jackson *et al.*, 2007). However, once the virus reaches the CNS, apoptosis may contribute to severe clinical neurological disease with a high mortality rate (Jackson *et al.*, 2006).

C. Spongiform Lesions

Spongiform lesions are round or oval vacuoles found in the grey matter neuropil of the CNS. They have been observed by Charlton and colleagues (1984, 1987, 1988) in skunks inoculated intramuscularly, intracerebrally and intranasally with several street rabies virus variants and in red foxes inoculated intramuscularly with a street virus

isolate. Charlton and colleagues (1984) also described similar findings in a small number of rabies-positive skunks, foxes, cows, horses and cats naturally infected with rabies. However, these findings are more typically associated with the transmissible spongiform encephalopathies (TSEs), which include scrapie, transmissible mink encephalopathy (TME), kuru and Creutzfeldt-Jakob disease (CJD) (Charlton, 1984). The spongiform changes of rabies are indistinguishable in size and shape at the light- and electron-microscope level from those observed in the TSEs (Charlton, 1984; Bundza and Charlton, 1988). However, the distribution of vacuoles is different. In rabies, spongiform changes are primarily found in the cerebral cortex and thalamus irrespective of the route of inoculation, virus variant or preparation of virus used, whereas in the TSEs there is a more widespread and variable distribution (Charlton *et al.*, 1987; Bundza and Charlton, 1988). The similarities between the spongiform lesions of rabies and the TSEs are suggestive of a common pathogenetic mechanism. It should be noted that spongiform changes are not a feature of human rabies.

The formation of spongiform lesions occurs at an early stage in rabies and advances rapidly. There is a progression from small to large membrane-bound vacuoles in cellular processes to large tissue spaces. The membrane-bound vacuoles occur primarily in dendrites and less commonly in axons and astrocyte processes (Charlton, 1984). The initial formation of these vacuoles is followed by a rapid enlargement within approximately 3 days which causes distention of the neuronal process and compression of the perivascular cytoplasm and adjacent neural tissue (Charlton *et al.*, 1987). Eventually, there is a disruption of the vacuolar membrane and the surrounding plasma membrane (Charlton, 1984; Charlton *et al.*, 1987). This produces the large spaces in the neuropil which often contain granular material and membrane fragments that originate from the

initial disruption of the membrane-bound vacuoles and the plasma membrane of the affected cellular processes (Charlton *et al.*, 1987). Cellular processes adjacent to the spongiform lesions often protrude into the cavity space and are known as peripheral blebs (Charlton, 1984; Charlton *et al.*, 1987).

The mechanism by which rabies virus infection causes spongiform lesions has yet to be determined. Charlton and colleagues have suggested that these lesions are produced via an indirect mechanism since rabies virions and matrix have only been found in neuronal processes in the vicinity of vacuoles, but not on the vacuolar membrane and only rarely in processes containing vacuoles (Charlton, 1984; Bundza and Charlton, 1988). This hypothesis is further supported by their observation of vacuolated areas that are devoid of rabies virus antigen (Charlton *et al.*, 1987). Vacuoles are also present in tissues with little or no perivascular cuffing (Charlton, 1984) and have been observed in immunocompromised skunks (Charlton *et al.*, 1987), arguing against the hypothesis that the lesions are due to an inflammatory reaction. One possible mechanism proposed by Charlton and colleagues is that a neurotransmitter imbalance may play a role in the formation of spongiform lesions (Bundza and Charlton, 1988). In particular, it has been hypothesized that the excitatory amino acids glutamate and aspartate possess excitotoxic properties and can produce lesions (dendrosomatotoxic/ axon-sparing) that are characterized by marked dendritic swelling (Olney *et al.*, 1979; Collins and Olney, 1982). Similar lesions can be produced by stimulation of cholinoceptive neurons, probably via indirect activity of glutamate and aspartate (Collins and Olney, 1982). Although the lesions produced by glutamate and aspartate are not identical to the spongiform lesions of rabies, the affinity for dendrites, the rapid progression and the ability to produce lesions remote from the site of stimulation led Charlton and co-workers to suggest a link between

these two process which should be explored further.

V. Damage or Dysfunction – What Causes the Neurological Disease in Rabies?

Under natural conditions, rabies virus infection of the CNS causes mild histopathological changes without prominent evidence of neuronal death despite its catastrophic clinical outcome. These findings have led to the idea that neuronal dysfunction, rather than neuronal death, is responsible for the clinical features and fatal outcome in natural rabies (Jackson, 2007; Fu and Jackson, 2005). It is known that some viruses can alter cellular functions without causing morphological changes to the host cell (Oldstone, 1984). In such cases, some of the differentiated functions of the cell suffer, while the vital functions remain intact. This ensures the survival of the cell, but results in specific functional disturbances. Some disturbances that have been suggested to play a role in rabies virus infection include ion channel dysfunction, abnormalities in neurotransmission, electrophysiological alterations, nitric oxide (NO) neurotoxicity and changes in gene expression and protein synthesis. However, no fundamental abnormality has been identified.

Ion channel dysfunction has been described in cultured neuroblastoma cells infected with the RC-HL strain of rabies virus using the whole-cell patch clamp technique (Iwata *et al.*, 1999). In particular, there was a reduction in the functional expression of ion channels responsible for voltage-dependent sodium currents and inward rectifier potassium currents. However, delayed rectifier potassium currents were not affected, suggesting that rabies virus infection does not cause non-specific dysfunction of ion channels. Voltage-dependent sodium channels and inward rectifier potassium channels play a role in generating the upstroke of action potentials and in determining the resting

membrane potential, respectively. As such, alterations in the expression of these channels were associated with a decrease in the resting membrane potential resulting from membrane depolarization, and could prevent host neurons from generating synaptic potentials or firing action potentials (Fu and Jackson, 2005). The outcome of these alterations could be an interference of neuronal transmission in infected neurons, resulting in functional impairment (Iwata *et al.*, 1999).

A number of studies have implicated abnormalities in acetylcholine (ACh) and serotonin (5-HT) neurotransmission in rabies virus infection. Tsiang (1982) described a reduction in the specific binding of quinuclidinyl benzylate (QNB), a ^{3}H-labeled antagonist, to muscarinic ACh receptors in CVS-infected rat brains, particularly in the hippocampus. Similar findings were observed in the hippocampus and brainstem of naturally infected rabid dogs (Dumrongphol *et al.*, 1996). However, Jackson (1993) found that the specific binding of ^{3}H-labeled QNB to muscarinic ACh receptors was not significantly different in the cerebral cortex or hippocampus of CVS-infected and mock-infected mice. Interestingly, Dumrongphol and colleagues (1996) reported a decrease in receptor affinity in the hippocampus of infected dogs even when rabies virus antigen was not observed. It has, therefore, been suggested that an unknown indirect mechanisms is responsible for the decreased receptor binding (Fu and Jackson, 2005).

Abnormalities in 5-HT binding and release have also been described in models of rabies virus infection. In the cerebral cortex of CVS-infected rats, maximum binding (B_{max}) of [^{3}H]5-HT to 5-HT$_{1}$ receptors was markedly decreased 5 days after peripheral inoculation (Ceccaldi *et al.*, 1993). In particular, this decrease was specific for 5-HT$_{1D}$-like receptors in this brain region. Furthermore, these decreases were observed before rabies virus antigen was detected, indicating again that the effect of rabies virus infection

on receptor binding is likely due to an indirect mechanism (Fu and Jackson, 2005). CVS infection also caused a decrease in the potassium-evoked release of [^{3}H]5-HT from virus infected synaptosomes in the cerebral cortex of peripherally inoculated rats compared to controls (Bouzamondo *et al.*, 1993)

Alterations of the electrophysiological properties of neurons have also been observed in rabies virus infection. Electroencephalographic (EEG) recordings from CVS-infected mice demonstrated three evolutionary phases during the progression of the disease (Gourmelon *et al.*, 1986). The initial phase exhibited changes in sleep stages, including rapid eye movement (REM) sleep disappearance, the emergence of pseudoperiodic facial myoclonus and the first clinical signs of disease. This was followed by a generalized EEG slowing (2-4 cycles/sec) in the mature phase, while the terminal phase coincided with the extinction of hippocampal rhythmic slow activity (RSA) and showed a flattening of cortical activity. The brain electrical activity ceased about 30 minutes before cardiac arrest. Alternatively, EEG recordings of street rabies virus-infected mice did not show any gross electrical abnormalities until a few hours before death (Gourmelon *et al.*, 1991). However, there were alterations of sleep stages at an early stage when clinical signs were absent, which included decreases in REM-sleep stages and increases in the duration of waking stages. The preservation of hippocampal RSA in CVS-infected mice and normal EEGs in street rabies-infected mice until late in the progression of the disease support the argument that neuronal death is not the mechanism of rabies virus lethality.

Nitric oxide (NO) toxicity has been proposed as a mechanism of neuronal dysfunction in rabies virus infection. Koprowski *et al.* (1993) reported that inducible nitric oxide synthase (iNOS) mRNA, the product of which catalyzes the production of

NO and is normally not detectable in the brain, was found in 3 of 7 street rabies virus infected mice displaying paralysis. The induction of iNOS mRNA occurred rapidly and coincided with the severity of clinical signs. iNOS was also detected in many cells, identified as macrophages, throughout the brain and particularly near blood vessels in CVS-infected rats (Van Dam *et al.*, 1995). Direct measurements of NO revealed a 30-fold increase in the brains of CVS infected rats compared to controls (Hooper *et al.*, 1995). Treatment of CVS-infected rats with aminoguanidine (AG), a selective inhibitor of iNOS, resulted in prolonged survival compared to controls (Ubol *et al.*, 2001). Furthermore, treatment with AG delayed rabies virus replication by 2 days.

Lastly, rabies virus infection has also been shown to have effects on cellular RNA and protein synthesis. Fu *et al.* (1993) reported that immediate-early-response genes (IEGs) encoding transcription factors are dramatically and specifically induced in particular regions of the hippocampus and cortex in CVS-infected rats. This increase in IEG mRNA coincided with the expression patterns of rabies virus RNA. On the other hand, levels of proenkephalin (pENK) mRNA and glyerceraldehye-3-phosphate dehydrogenase mRNA were reduced at terminal stages of the disease. Other host gene products that are significantly reduced at later stages of infection include the 5-hydroxytryptamine receptor (Ceccaldi *et al.*, 1993) and neuronal constitutive nitric oxide synthase (Akaike *et al.*, 1995). Prosniak *et al.* (2001) have estimated that approximately 90% of the genes detected in normal brains were down-regulated more than 4-fold in mice 6 days post-inoculation, whereas only 1.4% were up-regulated at this time.

VI. Damage to Neuronal Processes – Cause of Neuronal Dysfunction?

Li and colleagues (2005) used pathogenic and attenuated strains of rabies virus to

examine the structural integrity of neuronal processes *in vitro* and *in vivo* following infection. Silver staining of infected brain sections showed severe destruction and disorganization of the dendrites of hippocampal neurons in mice infected intracerebrally with the pathogenic strain, N2C, but not with the attenuated strain, SN-10, of rabies virus. However, hematoxylin-eosin (HE) staining revealed an opposite effect in the cell bodies of pyramidal neurons in the hippocampus. Pathological changes, including apoptosis, necrosis and neuronal loss, were observed in animals infected with SN-10, while those infected with N2C showed normal morphology.

Electron microscopy revealed similar findings. Hippocampal sections from N2C-infected mice showed low electron densities and the transverse or longitudinal sections of neuronal processes were no longer recognizable. Intracellular organelles, including the rough endoplasmic reticulum and free ribosomes, disappeared almost completely, while a few mitochondria were still visible. Furthermore, the number of synapses and presynaptic vesicles decreased compared to mock-infected and SN-10-infected mice. However, neuronal bodies in N2C-infected mice still showed normal morphologies, whereas there were early signs of apoptosis in SN-10-infected mice.

In order to investigate the mechanism of neuronal process degeneration, primary cortical neurons were stained for rabies virus antigen and cytoskeletal proteins, including microtubule-associated protein 2 (MAP-2) and neurofilament. Most neurons stained for viral antigen, but staining for the cytoskeletal proteins disappeared in primary neurons infected with pathogenic, but not attenuated rabies virus. Li and colleagues (2005) concluded that pathogenic rabies virus strains interrupt cytoskeletal integrity, thus disrupting neurotransmission and causing neuronal dysfunction. On the other hand, they suggested that attenuated rabies virus strains induce inflammation, which results in

neuronal apoptosis and necrosis (Miyamoto and Matsumoto, 1967).

VII. Is There a Role for Excitotoxicity in Rabies?

Another hypothesized mechanism of neuronal injury in rabies is excitotoxicity, or the pathological process by which neurons are damaged or killed by the over-activation of ionotropic receptors for the excitatory neurotransmitter glutamate, such as the N-methyl-D-aspartate (NMDA) receptor (Nargi-Aizenman *et al.*, 2004). There has been speculation that the NMDA receptor may be a rabies virus receptor. In mice infected with the challenge virus standard (CVS) strain of fixed rabies virus, the pattern of infection in the pyramidal neurons of the hippocampus while sparing of the granule cells in the dentate gyrus suggests that infection may be dependent on the presence of NMDA NR1 receptors (Gosztonyi and Ludwig, 2001). Furthermore, the non-competitive NMDA-receptor antagonists MK-801 and ketamine have been found to inhibit rabies virus infection *in vitro* and in the rat brain (Lockhart *et al.*, 1991; Tsiang *et al.*, 1991b; Lockhart *et al.*, 1992). This reduction in infection was attributed to the inhibition of viral genome transcription. The use of ketamine has been further supported as one of the agents given for the treatment of rabies with the survival of a case of rabies in which the patient did not receive immune prophylaxis, which was the first of its kind (Willoughby *et al.*, 2005). As such, it has been proposed that excitotoxicity may play a role in rabies virus infection.

Excitotoxicity is also believed to play a role in epilepsy, hypoxia-ischemia, Huntington's disease, stroke, amyotrophic lateral sclerosis and Alzheimer's disease (Xue *et al.*, 1994; Gill and Lodge, 1997; Lee *et al.*, 1999; Young, 1997; Weiss and Sensi, 2000; Oliva *et al.*, 2002). Furthermore, excitotoxicity has been found to play a role in some viral infections of the nervous system, including Sindbis virus encephalomyelitis and human

immunodeficiency virus infection (Nath *et al.*, 2000; Nargi-Aizenman *et al.*, 2001; Darman *et al.*, 2004).

Excitotoxicity is characterized by dendritic beading, or dendrotoxicity, and neuronal death. These pathological changes can be induced not only by glutamate, but also by glutamate analogs such as kainic acid (kainate), AMPA and NMDA, when administered via various routes, including subcutaneously, intraperitoneally and intraventricularly (Nadler *et al.*, 1977; Olney *et al.*, 1979; Ikegaya *et al.*, 2001). High concentrations of glutamate or its analogues result in neuronal death within minutes to hours, while lower concentrations cause dendritic beading within as little as 3 minutes (Koh *et al.*, 1990; Park *et al.*, 1996; Hasbani *et al.*, 1998). For example, application of kainate to cultured hippocampal slices invoked neuronal death selectively in area CA3 at concentrations in the range of 100-300μM, whereas it produced varicosities in all hippocampal sub regions at a low concentration of 30μM (Ikegaya *et al.*, 2001). Similar findings were found using NMDA and AMPA.

Dendrotoxicity is characterized by the formation of large swellings or "beads," which are separated from each other by thin dendritic segments, and preservation of the neuronal cell body (Olivia *et al.*, 2002). Beading is most commonly observed and is most severe in the hippocampus (Olney *et al.*, 1979). More specifically, beading appears to occur in dendritic branches distal to the site of excitation (Oliva *et al.*, 2002). In some cases beading is reversible, but in others beading irreversibly invades proximal dendritic segments and gradually encompasses the entire dendritic tree (Ikegaya *et al.*, 2001; Oliva *et al.*, 2002).

Electron microscopy of the hippocampus of rats treated with kainic acid intraperitoneally revealed areas of vacuolation which corresponded to dilated branches of

hippocampal dendrites (Olney *et al.*, 1979). These processes were empty except for variable amounts of particulate debris and an occasional degenerated mitochondrion. In hippocampal slice cultures exposed to NMDA, dendritic varicosities contained clear vacuoles and many short fragments of cytoskeletal elements, while the region between varicosities contained few organelles (Ikegaya *et al.*, 2001). Charlton (1984, 1987) has described similar findings in the neuropil of rabies virus-infected skunks. The neuropil microvacuolation that he observed consisted of membrane-bound vacuoles in dendrites which possess some similarities to excitotoxic amino acid-induced dendritic swelling.

It has been proposed that dendritic beading is a distinct feature of excitotoxicity that is not causally related to neuronal death, which is also an outcome of this pathological process (Ikegaya *et al.*, 2001). In studies of dissociated neocortical neurons and hippocampal explant slice cultures, the intracellular movement of sodium and chloride, but not calcium was found to produce dendritic beads (Hasbani *et al.*, 1998; Al-Noorie and Swann, 2000). Furthermore, dendritic beading has also been caused by the activation of voltage-gated sodium channels based on findings that veratridine, a voltage-sensitive sodium channel activator, effectively evoked varicosity formation, but did not cause signs of neuronal death (Oliva *et al.*, 2002). Neuronal death, on the other hand, is associated with excess intracellular calcium, which is mediated predominantly by NMDA receptor activation (Choi *et al.*, 1988). This glutamate-induced calcium influx results in the activation of phospholipases, oxidases, proteases and phosphatases, which leads to lethal metabolic derangement (Nicotera and Orrenius, 1998). This is further supported by the finding that NMDA-induced neuronal death, but not NMDA-induced dendritic beading, can be prevented by the use of calcium-free medium (Hasbani *et al.*, 1998; Ikegaya *et al.*, 2001). In contrast to NMDA-induced neuronal death, which is regionally

specific to area CA1 of the hippocampus in particular, dendritic swelling of hippocampal neurons occurs throughout the hippocampus. As such, Ikegaya and colleagues (2001) believe beading and neuronal death are two phenomena that are separable and involve distinct mechanisms. Furthermore, the finding that exposure of cultured hippocampal slices to low sodium conditions or proteinase inhibitors prevents varicosity formation, but aggravates NMDA-induced neuronal death suggests that beading may be associated with an early, self-protective response against excitotoxic death (Ikegaya *et al.*, 2001).

Proposed mechanisms of dendritic beading include water influx and cytoskeleton damage, both of which are believed to be the result of sodium entry into dendrites. Hasbani and colleagues (1998) observed an increase in dendritic volume following NMDA application to cortical cultures, which suggests the necessity of water and solute entry in varicosity formation. Sodium entry, followed by chloride entry to maintain electrical neutrality, may induce varicosity formation by drawing water across the dendritic plasma membrane in order to maintain osmotic balance (Al-Noori and Swann, 2000). This is supported by the finding that NMDA-induced varicosity formation in cortical cultures was attenuated in hypertonic media (Hasbani *et al.*, 1998).

Sodium, chloride and water entry may also lead to the disruption of cytoskeletal elements resulting in dendritic beading (Cornet *et al.*, 1988). Exposure of hippocampal slices to microtubule-depolymerizing agents colchicine and nocodazole or actin-depolymerizing agents cytochalasin D and latrunculin A produce dendritic beading, but not neuronal death (Ikegaya *et al.*, 2001). Similarly, fragmented microtubules have been observed in NMDA-induced dendritic varicosities in cortical neurons (Emery and Lucas, 1995) and beaded dendrites of human cortical biopsies (Purpura *et al.*, 1982). Transient NMDA exposure of hippocampal slices is also associated with the loss of microtubule

associated protein 2 (MAP-2) from dendrites (Hoskison and Shuttleworth, 2006; Hoskison *et al.*, 2007). These findings suggest that sodium influx may activate proteases which could result in cytoskeletal protein degradation. This is supported by the finding that co-application of NMDA and a cocktail of protease inhibitors significantly attenuated varicosity formation in cultured rat hippocampal slices (Ikegaya *et al.*, 2001). The end result of cytoskeletal degradation is the accumulation of organelles and cytoplasm in regions where microtubule loss is sufficient enough to interrupt cytoplasmic transport, ultimately causing varicosity formation (Emery and Lucas, 1995)

CHAPTER 2: THESIS OBJECTIVES

The events in rabies virus infection that lead to CNS disease and a fatal outcome are still not well understood. Under natural conditions, rabies virus infection causes mild histopathological changes without prominent evidence of neuronal death despite its lethality. These observations suggest that virus-induced neuronal dysfunction, rather than neuronal death, is the basis for the acute and fatal neurological infection (Fu and Jackson, 2005). We have hypothesized that excitotoxicity with NMDA receptor activation plays an important role in the pathogenesis of rabies. In order to investigate the basis of neuronal dysfunction, the morphological changes in neuronal processes of transgenic mice (C57BL background) expressing the yellow fluorescent protein (YFP) in neurons were characterized after rabies virus infection. Furthermore, the role of NMDA receptor activation in rabies virus infection was explored in mice infected intracerebrally or by a peripheral route with CVS and treated with ketamine, a non-competitive NMDA receptor antagonist, or vehicle.

CHAPTER 3: MATERIALS AND METHODS

I. Virus

The challenge virus standard (CVS-11) strain of fixed rabies virus, which was obtained from Dr. William H. Wunner (The Wistar Institute, Philadelphia, PA.), was used in these studies.

II. Animals and Inoculations

Ketamine Study

Six-week-old female ICR mice (Charles River Canada, St. Constant, Quebec) were inoculated either intracerebrally with 857 PFU or in the right hindlimb footpad with 3.0×10^6 PFU of CVS in 0.03mL (intracerebral, $n = 36$; footpad, $n = 54$). Uninfected controls were inoculated with vehicle, phosphate-buffered saline (PBS), in the same manner (intracerebral, $n = 6$; footpad, $n = 6$). Half of the infected mice and half of the controls were given 60mg/kg ketamine (Pfizer, Kirkland, QC) in 0.05mL PBS (vehicle) intraperitoneally every 12 hours, which anesthetized the mice for a short period of time. The remaining mice received 0.05mL PBS intraperitoneally every 12 hours. Clinical signs of disease, including limb weakness and paralysis, were recorded daily and mice were euthanized at early time points or once moribund to compare the progression of disease and mortality between treatment groups.

Study in YFP Mice

Six to 7-week-old male and female transgenic mice (C57BL background) expressing yellow fluorescent protein (YFP) in neurons (H-line) were inoculated in the right hindlimb footpad with 3.1×10^7 PFU of CVS in 0.03mL or mock-infected in a

similar manner (virus-infected, $n = 23$; mock-infected $n = 21$). The original colony of mice was created by Feng and colleagues (2000). In this study, B6.Cg-Tg(Thy1-YFP)16Jrs/J male mice (The Jackson Laboratory) were mated with C57BL female mice (Charles River Canada, St. Constant, Quebec). In subsequent matings, male offspring expressing YFP in neurons (YFP positive) were mated with YFP negative females. YFP positive mice of the H-line express the protein predominantly in layer V of the cerebral cortex, in mossy fibers of the cerebellum and in dorsal root ganglia (Feng *et al.*, 2000). There is no expression in the Purkinje cells or molecular layer of the cerebellum.

Each procedure involving the use of animals was subject to the review and approval by the Queen's University Animal Care Committee. All animals were housed and manipulated in accordance to the Canadian Council on Animal Care Guidelines.

III. Preparation of Tissue Sections

Ketamine Study

ICR mice were anesthetized with isoflurane and perfused with buffered 4% paraformaldehyde between days 3 to 6 post-infection (p.i.), or after they developed clinical rabies and became moribund. Of those mice inoculated intracerebrally, 4 mice in each treatment groups were perfused on day 3 and day 5 p.i. for evaluation of early time points. The remaining 20 mice, two of which did not develop clinical disease in the vehicle treatment group, were perfused once moribund. In the footpad inoculation group, 4 mice from each treatment group were perfused on each of days 3 through 6 p.i. for early time point evaluation. The remaining 22 mice, one of which did not develop clinical disease in the vehicle treatment group, were perfused once moribund. One intracerebrally and one footpad mock-infected mouse from each treatment group was perfused on day 3,

7 or 9 p.i. Brains were removed and immersion-fixed in the same fixative for 24 h at 4°C. Tissue was dehydrated and embedded in paraffin (Fisher Scientific, Ottawa, ON) using a Tissue-Tek tissue embedding console system (Miles Laboratories, Mishawaka, IN). Coronal tissue sections (6μm) were prepared on a Microtome 2030 Biocut (Reichert-Jung, Germany) and mounted onto SuperFrost slides (Fisher Scientific, Ottawa, ON) for cresyl violet and immunohistochemical staining.

Study in YFP Mice

YFP transgenic mice (YFP mice) were anesthetized with isoflurane and perfused with modified Karnofsky's fixative (2.5% glutaraldehyde and 2% paraformaldehyde in 0.1M cacodylate buffer) once they became moribund (virus infected, $n = 3$; mock infected, $n = 3$) or with buffered 4% paraformaldehyde once they developed hindlimb paralysis (virus infected, $n = 5$; mock infected, $n = 5$) or after they became moribund (virus infected, $n = 15$; mock infected, $n = 13$). Brains were removed and immersion-fixed in the same fixative for 24 h at 4°C. Tissues from 7 moribund mice and 6 mock-infected mice perfused with 4% paraformaldehyde were embedded in paraffin and sectioned as described above for histological and immunohistochemical studies using light microscopy. The tissue from those mice perfused with modified Karnofsky's fixative was embedded in plastic for toluidine blue staining and electron microscopy. Coronal sections (50μm) of various brain regions from the remaining mice were cut on a Leica VT 1000S vibratome (Leica, Germany) and either stored in 16 well plates in PBS at 4°C for fluorescent rabies virus antigen staining or transferred to SuperFrost slides and coverslipped with Polymount (Polysciences, Warrington, PA) for morphological studies using fluorescent microscopy.

IV. Cresyl Violet Staining

Paraffin embedded tissue sections were deparaffinized by heating in an oven at 60°C for 10 minutes and subsequently immersed in Histoclear (Diamed Lab Supplies, Mississauga, ON) for 2 minutes. Tissue was rehydrated by successive immersion in 100% ethanol, 95% ethanol, 70% ethanol and distilled water (dH_2O) for 2 minutes each. Slides were stained with cresyl violet for 5 minutes and rinsed in PBS for 2 minutes. This was followed by immersion in 70% ethanol, 95% ethanol, 95% ethanol with 2mL of glacial acetic acid, 95% ethanol and 100% ethanol until the desired colour was achieved and then Histoclear for 2 minutes. Slides were then coverslipped with Permount (Fisher Scientific, Fair Lawn, NJ).

Morphological changes of apoptosis were evaluated in neurons stained for cresyl violet in the cerebral cortex and hippocampus (CA1 and CA3 regions) of ICR mice inoculated intracerebrally and compared between ketamine and vehicle treatment groups using light microscopy (40x objective). A semiquantitative evaluation of the severity of apoptotic changes was performed on day 3 p.i. (vehicle, n=4; ketamine, n=4) or day 5 p.i. (vehicle, n=4; ketamine, n=3) or once mice were moribund (vehicle, n=3; ketamine, n=6) with the following scheme: 0, no significant changes; 1, mild changes; 2, moderate changes; 3, severe changes; and 4, very severe changes and/or neuronal loss. The identity of all slides was masked during scoring in order to prevent bias in the evaluation.

A histological examination of the cerebral cortex and area CA1 of the hippocampus in YFP tissue sections was also performed. A comparison was made between tissues from infected and mock-infected YFP animals.

V. Hematoxylin and Eosin Staining

Paraffin embedded tissue sections from YFP mice were deparaffinized and rehydrated as previously described. The sections were stained with Harris Modified Hematoxylin for 5 minutes then dipped in water 10 times, acid alcohol 3 times and again in water 10 times. Prior to counterstaining the tissue sections with Eosin working solution for 8 minutes, the tissue was washed in tap water substitute for 2 minutes and water for 5 minutes. Lastly, the tissue was dehydrated by dipping the slides 3 times in 95% ethanol, 5 times in 100% ethanol and then immersing the slides in 100% ethanol for 2 minutes. The slides were immersed in Histoclear for 4 minutes prior to being coverslipped with Permount. A histological examination of the cerebral cortex and area CA1 of the hippocampus was performed. A comparison was made between tissue from infected and mock-infected YFP animals.

VI. Immunohistochemistry

A. Rabies Virus Antigen Staining - EnVision Method

Paraffin embedded tissue sections were stained for rabies virus antigen using the EnVision method. Slides were deparaffinized and rehydrated as previously described. Slides were incubated in 1.0% H_2O_2 in MeOH for 30 minutes and rinsed twice in PBS for 1 minute prior to treatment with monoclonal mouse anti-rabies virus nucleocapsid protein IgG 5DF12 diluted 1:160 overnight at room temperature (obtained from Alexander I. Wandeler, Centre of Expertise for Rabies, Canadian Food Inspection Agency, Nepean, Ontario). Slides were rinsed twice in PBS for 1 minute prior to application of DakoCytomation EnVision+ System-HRP labeled polymer anti-mouse secondary antibody (DakoCytomation, Denmark) for 40 min. After rinsing in PBS twice for 1

minute, slides were incubated in 0.5mg/mL 3,3-diaminobenzidine tetrachloride (DAB; Polysciences, Warrington, PA) in 0.01% H_2O_2 in PBS for 8 minutes. Slides were rinsed twice in PBS for 2 minutes, incubated in 0.5% $CuSO_4$ in 0.15M NaCl for 5 minutes, and rinsed in tap water twice for 1 minute. Tissues were counterstained with Gill's hematoxylin for 1 minute, rinsed in tap water for 1 minute, tap water substitute for 2 minutes and tap water for 1 minute. Sections were then dehydrated by successive immersion in 70% ethanol, 95% ethanol and 100% ethanol for two minutes each. After immersion in Histoclear for 2 minutes, sections were coverslipped with Permount.

Rabies virus infection was evaluated in the midbrain tegmentum, cerebral cortex and hippocampus (CA1 and CA3 regions) of ICR mice inoculated intracerebrally or in the right hindlimb footpad in both the ketamine and vehicle treatment groups. Slides stained for rabies virus antigen from mice perfused on days 3 through 6 (n=4 in each treatment group on each day, except n=3 on day 5 in the intracerebrally inoculated ketamine-treated group) or moribund mice (intracerebrally inoculated: vehicle, n=3; ketamine, n=6 / footpad-inoculated: vehicle, n=8; ketamine, n=11) were blinded and the numbers of infected neurons were counted in three different fields with the most marked staining within the same brain region using high power (40x) objective. The average number of infected neurons was compared between treatment groups for each early time point and in moribund mice.

Rabies virus infection was also evaluated in the cerebral cortex and area CA1 of the hippocampus of moribund YFP mice. Staining in infected and mock-infected tissues was compared.

B. Rabies Virus Antigen Staining - Fluorescent Method

Floating tissue sections (50μm) from YFP mice were stained for rabies virus antigen using Alexa Fluor 568 goat anti-mouse IgG (H+L) fluorescent secondary antibody (Molecular Probes, Eugene, OR), which fluoresces red. Tissue sections were stained in 16 well plates using a nutating mixer to ensure exposure of tissue to the reagents. Sections were first washed in PBS for 10 minutes prior to incubation with 0.3% H_2O_2 in 50 % MeOH for 30 minutes. Sections were washed 3 times in PBS for 10 minutes and then blocked in 10% normal goat serum (NGS) for one hour prior to the application of monoclonal mouse anti-rabies virus nucleocapsid protein IgG 5DF12 diluted 1:200 for 48 hours at 4°C. Sections were washed three times in PBS for 10 minutes and then incubated for 18 hours at 4°C in Alexa Fluor 568 goat anti-mouse IgG (H+L) diluted 1:800. The secondary antibody was centrifuged for 5 minutes prior to use and only the supernatant was used in the dilution. After the secondary antibody was added, the plates were covered with aluminum foil to reduce exposure to light. Sections were then washed three times in 0.2% Triton X-100 and once in PBS for 10 minutes each time. Sections were transferred to SuperFrost slides and allowed to partially dry before being coverslipped with Polymount. The rabies virus antigen staining was viewed using a N21 fluorescent filter and compared between infected and mock-infected YFP mice.

C. Caspase-3 Staining

Paraffin embedded tissue sections from YFP mice were deparaffinized and rehydrated as previously described. Slides were microwaved in a 10mM sodium citrate and 0.05% Tween 20 solution (pH 6) for 1 minute on high power and 9 minutes on medium power, and then cooled for 20 minutes prior to being rinsed twice in PBS. The

tissue was blocked for 20 minutes with 5% NGS in PBS and then rinsed 3 times in PBS with 0.1% Tween 20. Cell Signalling anti-cleaved caspase-3 primary antibody, diluted 1:200 in PBS with 2% NGS, was applied to the slides overnight in a humidity chamber at room temperature. Tissues were washed twice in PBS with 0.1% Tween 20 and the secondary biotinylated goat anti-rabbit antibody diluted 1:100 in PBS with 2% NGS was applied for 30 minutes. Slices were then washed in PBS with 0.1% Tween 20 three times before quenching the endogenous peroxidases with 1% H_2O_2 in MeOH for 30 minutes. After washing the sections twice in PBS with 0.1% Tween 20, they were incubated with ABC reagent for 30 minutes and again washed twice in PBS with 0.1% Tween 20 prior to incubation with 0.5mg/mL DAB in PBS containing 0.01% H_2O_2 for 8 minutes. Next, slices were rinsed twice in tap water, incubated in 0.5% $CuSO_4$ in 0.15M NaCl for 5 minutes, rinsed twice in tap water and counterstained in hematoxylin for 1 minute. Lastly, the tissue was rinsed twice in tap water, tap water substitute for 3 minutes, twice in tap water again and then dehydrated by successive immersion in 70% ethanol, 95% ethanol and 100% ethanol for two minutes each. After immersion in Histoclear for 4 minutes, sections were coverslipped with Permount. Caspase-3 staining was compared in the cerebral cortex and area CA1 of the hippocampus from infected and mock-infected YFP mice.

VII. Terminal Deoxynucleotidyl Transferase Mediate dUTP Nick End Labeling (TUNEL) Staining

Paraffin embedded tissue sections from YFP animals were deparaffinized and rehydrated as previously described. Slides were microwaved in 10mM citrate buffer (pH 3) for 1 minute on high power and 9 minutes on medium power, and then cooled for 20

minutes before rinsing twice in PBS for 2 minutes. Sections were next incubated in 15μg/mL Proteinase K (Sigma) in 10mM Tris (pH 8) for 15 minutes then rinsed twice in dH_2O for 2 minutes. For positive controls, slides were equilibrated in DN buffer (30mM Tris, 4mM $MgCl_2$, 0.1mM dithiothreitol) for 5 minutes, incubated in 1μL/mL DNase (Pharmacia) in DN buffer for 10 minutes and rinsed five times in dH_2O for 3 minutes. Next, endogenous peroxidases were quenched in 3% H_2O_2 in PBS for 5 minutes. Sections were rinsed twice in dH_2O for 5 minutes then blocked in 1X blocking solution (Boehringer Mannheim) for 20 minutes in a humid chamber at room temperature. Slides were washed twice in PBS for 2 minutes prior to equilibration in terminal transferase (TdT) buffer (5x buffer is 1M sodium cacodylate and 150mM Tris pH 6.6 with bovine serum albumin) for 5 minutes and incubated in TdT enzyme solution (20μL 5x TdT buffer, 4μL 25mM $CoCl_2$, 0.24μL Biotin-16-dUTP (Roche), 75.72μL dH_2O and 0.04μL TdT enzyme (Roche)) for 60 minutes in a reaction chamber at 37°C. This reaction was stopped by placing the slides in a 300mM sodium chloride and 30mM sodium citrate solution (pH 7.2) for 45 minutes. Sections were rinsed twice in PBS for 2 minutes before applying the Vectastain Elite ABC reagent (prepared 30 minutes before use) for 30 minutes in a humid chamber. Slides were again rinsed twice in PBS for 2 minutes then incubated in 0.5mg/mL DAB in PBS containing 0.01% H_2O_2 for 8 minutes and rinsed twice in tap water for 2 minutes. Tissue was counterstained with methyl green (2% in 0.1M sodium acetate pH 4.2) for 10 minutes, quickly rinsed with 2 dips in ice cold dH_20, then rinsed in three changes of butanol for 3 dips, 3 dips and 2 minutes. Lastly, slides were immersed in Histoclear for 4 minutes then coverslipped with Permount. TUNEL staining was compared in the cerebral cortex and area CA1 of the hippocampus from infected and mock-infected YFP mice.

VIII. Bielschowsky Silver Staining

Paraffin embedded tissue sections from YFP mice were deparaffinized and rehydrated as previously described. Slides were incubated in 50mL of 20% silver nitrate solution (20mg silver nitrate, 100mL dH_20) for 30 minutes at 37°C in the dark. Slides were then placed in dH_2O while concentrated ammonium hydroxide was added drop by drop to the 20% silver nitrate solution until the initial precipitate disappeared. Next, slides were returned to the silver nitrate solution for 15 minutes in the dark. Two drops of concentrated ammonium hydroxide were added to 50mL of dH_2O and used to wash the slides. Two or three drops of developer (20mL 37% unbuffered formalin, 100mL dH_2O, 100µl concentrated nitric acid, 0.5mg citric acid) were added to the silver nitrate solution and this solution was used to stain the slides for 3-5 minutes. Lastly, slides were washed in dH_2O, fixed in 5% aqueous sodium thiosulfate (5mg sodium thiosulfate, 100mL dH_2O) for 1-5 minutes and washed well in several changes of distilled water before being dehydrated and coverslipped with Permount. Silver staining was compared in the cerebral cortex of infected and mock-infected YFP mice.

IX. Fluorescent Microscopy

Morphological features of beading were evaluated in neurons expressing YFP in vibratome sections of the cerebral cortex, hippocampus, cerebellum and brainstem from virus-infected moribund mice perfused on days 9 through 12 p.i. and mice with right hindlimb paralysis perfused on day 6 p.i. using an I3 fluorescent filter and a Leica fluorescent microscope and compared to mock-infected YFP mice. The percentage of affected dendrites and axons was quantified separately in the cerebral cortex of moribund and control mice (virus-infected, n=5; mock-infected, n=5). Slides were masked and the

total number of dendrites or axons and the number of dendrites or axons displaying signs of beading or fragmentation were counted in three different fields using high power (25x) objective. The average number of affected dendrites or axons was divided by the average number of total dendrites or axons to determine the percentage of dendrites or axons (± standard error of the mean) with abnormal morphology. Sections of the various brain regions in mice with right hindlimb paralysis were examined in order to describe the morphological changes in neuronal processes at an early time point (day 6 p.i.) in the progression of infection. Fluorescent microscopy was also used to identify the nuclei of origin of the cerebellar mossy fibers.

X. Toluidine Blue Staining

Tissues from YFP mice perfused with Karnofsky's fixative were dissected after being immersion-fixed in the same fixative for 24 h at 4°C. Sections of the frontal cortex, area CA1 of the hippocampus and cerebellum from all 6 mice were then immersed in 1% osmium tetroxide, dehydrated by successive immersion in 70% ethanol, 85% ethanol, 95% ethanol and 100% ethanol, cleared with propylene oxide and infiltrated with resin (Jembed resin; J.B. EM Services, Dorval, Quebec). Sections (1μm thick) were stained with toluidine blue and examined using light microscopy. The percentage of pyramidal neurons displaying cytoplasmic vacuolation in layer V of the cerebral cortex and in area CA1 of the hippocampus were quantified (Cortex: virus-infected, n=3; mock-infected, n=3/ CA1: virus-infected, n=2; mock-infected, n=3). Slides were masked and the total number of neurons and the number of neurons displaying signs of cytoplasmic vacuolation were counted in three different fields using high power objective (cortex, 40x; CA1, 100x). The average number of affected neurons was divided by the average

number of total neurons to determine the percentage of neurons (± standard error of the mean) with cytoplasmic vacuolation in CVS-infected and mock-infected YFP mice.

XI. Electron Microscopy

Ultrathin sections were cut from four resin-embedded samples of the frontal cortex, two infected and two mock-infected. Sections were stained with uranyl acetate and lead citrate and examined with an electron microscope (Hitachi H7000; Hitachi, Schaumburg, Illinois, USA) at 75 kV.

XII. Statistical Analyses

Clinical disease and mortality data from ketamine and vehicle-treated intracerebrally and footpad inoculated ICR mice were analyzed using Kaplan-Meier survival curves and log rank tests. T-tests for the significance of the difference between the means of two samples were used to compare the number of rabies virus infected neurons between ketamine and vehicle treatment groups in intracerebrally and footpad inoculated ICR mice and the percentage of cortical and hippocampus pyramidal neurons displaying beading/fragmentation or cytoplasmic vacuolation between mock-infected and virus-infected YFP mice. Mann Whitney tests for the significance between two independent samples were used to compare the severity of apoptosis between ketamine and vehicle treatment groups in intracerebrally inoculated ICR mice. A value of $p<0.05$ was considered statistically significant.

CHAPTER 4: RESULTS

I. Evaluation of the Effects of Ketamine in Rabies Virus Infected Mice

A. Clinical Observations

Mice infected in the right hindlimb footpad with CVS and treated with either ketamine or vehicle developed hindlimb paralysis between days 5 and 6 p.i. Over the next 3 days there was progression to quadriparesis and all surviving mice became moribund by day 9 p.i. A logrank test indicated that there was no difference in the onset or progression of disease (Fig. 1A, $p=0.54$), or in the mortality rate between mice that received ketamine or vehicle (Fig. 1C, $p=0.53$).

Mice infected intracerebrally with CVS began to display signs of rabies, including ataxia and paralysis, on day 6 p.i., and were all affected by day 8 p.i. in the ketamine treatment group and by day 7 p.i. in the vehicle treatment group. There was no significant difference in the onset or progression of disease between mice that received ketamine or vehicle as determined by a logrank test (Fig. 1B, $p=0.30$). All mice treated with ketamine were moribund by day 9 p.i., and those treated with vehicle by day 8 p.i. Again, a logrank test indicated no difference in the mortality rate between treatment groups (Fig. 1D, $p=0.50$).

B. Rabies Virus Antigen Distribution

Mice inoculated in the right hindlimb footpad displayed few neurons staining for rabies virus antigen in the midbrain tegmentum on day 3 p.i. in the ketamine treatment group. On day 4 p.i., antigen was observed in the midbrain tegmentum of both treatment groups, and in the cerebral cortex of mice treated with vehicle, while mice treated with ketamine first displayed antigen in the cerebral cortex on day 5 p.i. By day 6 p.i., the

number of infected neurons increased in the midbrain tegmentum and cerebral cortex of both treatment groups, and infection first appeared in areas CA1 and CA3 of the hippocampus. A comparison of the number of infected neurons in the various brain regions between treatment groups on days 3 through 6 p.i. did not show a significant difference (Table 1, $p>0.05$ for all brain regions). Similarly, there was no difference in the amount of infection in the cerebral cortex (Fig. 3A and B) or areas CA1 and CA3 (Fig. 3C and D) of the hippocampus between treatment groups in tissue from moribund mice inoculated in the footpad (Fig. 2A, $p>0.05$). However, there was a greater number of infected neurons in the midbrain tegmentum of moribund mice treated with ketamine compared to vehicle (Fig. 2A, $p=0.0009$; Fig. 3E and F).

Mice inoculated intracerebrally in both treatment groups displayed rare but comparable virus antigen staining in the cerebral cortex, area CA1 of the hippocampus and midbrain tegmentum on day 3 p.i. Area CA3 of the hippocampus was more heavily stained than other regions on day 3 p.i., but was similar between treatment groups (Table 1, $p>0.05$ for all brain regions). By day 5 p.i. the number of infected neurons in all areas had markedly increased, but there was no difference between treatment groups (Table 1, $p>0.05$ for all brain regions). This finding was also observed in tissue from moribund mice in both treatment groups (Fig. 2B, $p>0.05$ for all brain regions).

C. Histopathological Changes

Very mild morphological changes of apoptosis, including cytoplasmic shrinkage and nuclear condensation, were observed in the cerebral cortex of mice inoculated intracerebrally and treated with ketamine on day 5 p.i., but not in mice treated with vehicle. Mild apoptotic changes were also observed in area CA1 of the hippocampus in

both treatment groups on day 5 p.i. Hippocampal subfield CA3 showed more moderate changes of apoptosis in both treatment groups on this day.

Tissues from moribund mice in both treatment groups displayed only mild to moderate changes of apoptosis in the cerebral cortex. Extensive apoptotic cell death and cell loss were observed in areas CA1 and CA3 of the hippocampus, particularly in the vehicle treatment group (Fig. 3G and H). Comparisons of the two treatment groups using a Mann Whitney test indicated that there was no significant difference in the severity of apoptosis between treatments at any time point (Table 2, $p>0.05$).

II. Evaluation of the Structural Integrity of Neuronal Processes in Rabies Virus Infected YFP Transgenic Mice

A. Rabies Virus Antigen Distribution

Staining for rabies virus antigen in paraffin embedded tissue sections revealed widespread infection of neurons in the cerebral cortex (Fig. 4A) and hippocampus (Fig. 4C) of CVS-infected YFP moribund mice. In both of these regions antigen was found in the perikarya of pyramidal neurons and in the dendritic processes. Control tissues showed low background staining (Fig. 4B and D).

B. Histopathological Changes

Pathological changes were minimal in paraffin embedded tissue sections stained for cresyl violet and hematoxylin and eosin (HE). The predominant findings were inflammatory changes in the leptomeninges and parenchyma and perivascular cuffing. Activated microglia were observed throughout the cerebral cortex, in areas CA1 and CA3 of the hippocampus and surrounding blood vessels in both of these regions (Cortex, Fig.

5A and C; CA1, Fig. 6A and C). Low grade inflammation was also observed in the leptomeninges. Overall, there was no well defined cytopathology in pyramidal neurons under light microscopy.

Pathological findings were more evident in the cerebellum. Activated microglia were abundant, especially in the molecular layer. The leptomeninges also displayed increased inflammation in comparison to the leptomeninges of the cerebral cortex. HE staining also revealed vacuolation in the deep cerebellar white matter (Fig. 7A).

C. Caspase-3 and TUNEL Staining

Caspase-3 and TUNEL staining revealed little evidence of apoptosis in the cerebral cortex and hippocampus of moribund YFP mice. Caspase-3 staining was rarely observed in the cerebral cortex of these animals, and this very mild staining was in non-neuronal cells (Fig. 8A). The hippocampus of moribund animals (Fig. 8C) and the cerebral cortex and hippocampus of control mice showed low background staining (Fig. 8B and D).

TUNEL staining was increased compared to caspase-3 staining, but was still only observed in few cells in the cerebral cortex of moribund YFP mice (Fig. 9A). There was also rare TUNEL staining in area CA1 of the hippocampus (Fig. 9D). Positive controls for oligonucleosomal DNA fragmentation, which were pre-treated with DNase, revealed widespread TUNEL staining throughout the cerebral cortex (Fig. 9C) and hippocampus (Fig. 9F) of moribund YFP mice, while tissues from mock-infected mice showed low background staining (Fig. 9B and E).

D. Fluorescent Microscopy

Studies using fluorescent microscopy revealed morphological abnormalities in neuronal processes expressing YFP in regional brain areas of moribund mice (perfused on days 9 through 12 p.i.), including the cerebral cortex, brainstem, hippocampus and cerebellum. Analysis of these same brain regions at an early time point (day 6 p.i.) in mice with right hindlimb paralysis revealed only minor changes in selective regions. The variation in severity of these abnormalities did not only exist between the two different time points, but also between different brain regions at a given time point. In moribund animals, the changes in affected processes ranged from interspersed swellings on intact processes, also known as beading, to severely distended sections of neuronal processes without apparent physical connections between the residual swollen pieces (fragmentation). Processes that displayed beading were also characterized by inter-bead segments that were thinner than neuronal processes in mock-infected tissue.

Mice with hindlimb paralysis displayed very minor morphological changes in processes of the cerebral cortex, hippocampus and cerebellum and no abnormalities in the perikarya in these regions. Distal dendrites of pyramidal neurons in the cerebral cortex (Fig. 10A) and area CA1 of the hippocampus displayed extremely rare beading in one of five animals. Rare beading was also observed in axons in the cerebral cortex of four of five animals (Fig. 10C). The mossy fibers of the cerebellum were most noticeably affected with minor beading occurring primarily in the cerebellar commissure, which connects the two hemispheres of the cerebellum (Fig. 10E). The more obvious involvement of the cerebellum is consistent with the sequential infection of the cerebellum that is followed by infection of the cerebral cortex then hippocampus after footpad inoculation (Jackson and Reimer, 1989). However, examination of fluorescent

rabies virus antigen staining at this time point also revealed widespread staining in the cerebral cortex (Fig. 11A). Antigen staining in area CA1 of the hippocampus was minimal and varied in intensity between animals.

In the cerebral cortex of moribund mice, the dendrites of many layer five pyramidal neurons exhibited marked structural abnormalities, while relatively few perikarya showed structural changes. Rare perikarya were shrunken, whereas 12.2 ± 2.7% of dendrites showed beading and fragmentation in CVS-infected mice (Fig. 12A, C and E) versus 0% of dendrites in mock-infected mice ($p=0.01$). Dendrites in mock-infected mice were characterized by a gradual tapering in diameter from the proximal dendrite to the distal dendrite (Fig. 12B, D and F). The axons of pyramidal neurons were more involved but displayed less severe morphological abnormalities than the dendrites, primarily displaying signs of beading and, to a lesser extent, fragmentation in 40.5 ± 7.8% of axons in infected tissues (Fig. 12G) vs. 2.4 ± 1.2% of axons in mock-infected tissues ($p=0.002$; Fig. 12H). Axons in control cortical tissues were slightly varicose, but this is characteristic of these processes.

Fluorescent microscopy was also used to examine the fluorescent rabies virus antigen staining in the cerebral cortex of moribund mice, which confirmed widespread infection of cortical neurons (Fig. 11B). It was not possible to identify the cell bodies of beaded or fragmented neuronal processes staining for rabies virus antigen or vice versa since the sections were only rarely cut in a plane with visualization of a complete neuron and, in addition, fragmentation of dendrites made it difficult to follow their course.

Mossy fibers in the cerebellum of moribund animals showed severe fragmentation in the majority of axons within the cerebellar commissure (Fig. 13A), and less severe beading in the white matter of the folia. Beading was also observed in the granular layer

of the cerebellum where extensions of the mossy fibers synapse with granule cells (Fig. 13C). The granule cells themselves did not display any morphological abnormalities, but there was variability in the size and shape of these cells in control mice which made it difficult to identify subtle pathological changes. Mossy fibers in control tissues are also varicose and vary in diameter, but these features are distinct from the beading and fragmentation observed in infected tissues (Fig. 13B and D).

Axons were also involved at various levels in the brainstem of moribund mice. In particular, the tracts traveling rostral-caudally through the central brainstem, which include the tectobulbar tract and the medial longitudinal fasciculus, displayed distended and fragmented axons of varying degrees of severity (Fig. 14A and C). In some tissue samples it seemed that there was also a loss of neuronal processes in this region compared to controls (infected, Fig. 14C; control, Fig. 14D). Another area which consistently showed signs of beading involved the fibers of the inferior cerebellar peduncles, some of which become the mossy fibers of the cerebellum (Fig. 14E). Mossy fibers originate as axons emerging from a number of nuclei in the brainstem and spinal cord, including the pontine nucleus, vestibular nuclei, lateral reticular nucleus, spinal trigeminal nucleus and the external cuneate nucleus, then travel towards the cerebellum (Yatim et al., 1996; Rodriguez and Dymecki, 2000). Although the major source of the cerebellar mossy fibers is known to be the pontine nuclei, the cell bodies of these nuclei did not express YFP in these animals (Fig. 14G). Examination of the nuclei which do express YFP in the brainstem revealed that a probable source of the mossy fibers expressing YFP are the vestibular nuclei (Fig. 14H). Axons emerging from these nuclei displayed severe fragmentation as they traveled into the cerebellum. Staining of tissue sections containing the vestibular nuclei for fluorescent rabies virus antigen indicated that some of these cell

bodies are infected, but not a majority. It is likely that additional nuclei in the spinal cord or caudal brainstem express YFP and contribute to the mossy fibers because of involvement of fibers in the inferior cerebellar peduncle.

In contrast to the findings in other brain regions of moribund mice, area CA1 of the hippocampus showed very few structural abnormalities (Fig. 15A) despite extensive rabies virus infection (Fig. 4C, Fig. 11C). In most cases, infected tissues were morphologically indistinguishable from control tissues (Fig. 15B). Abnormal shrunken perikarya of CA1 pyramidal neurons were rare (Fig. 15C and D). Even more uncommon were changes in the distal dendrites, which took the form of mild dendritic beading. There were no observable abnormalities in the axons of CA1 pyramidal neurons.

E. Bielschowsky Silver Staining

Silver staining revealed changes in a minority of axons in the cerebral cortex of moribund YFP mice in comparison with mock-infected cortices. These rare axons displayed minor degrees of beading and an undulating course as they traveled from the neuron cell bodies to the deep white matter of the cortex (Fig 16A).

F. Toluidine Blue Staining

Morphological evaluation of the cerebral cortex, area CA1 of the hippocampus and cerebellum in toluidine blue-stained sections of moribund YFP mice revealed vacuoles within neuronal cell bodies and processes in addition to larger vacuolation within neuropil. In pyramidal neurons of the cerebral cortex in CVS-infected mice, numerous irregular round vacuoles were observed within the cytoplasm of the perikarya and in the proximal dendrites (Fig. 17C, D and E). The vacuoles caused distention of the

area occupied by the cytoplasm. On average, 60.8 ± 8.5% of pyramidal neurons in CVS-infected mice showed such abnormalities while only 1.0 ± 0.2% did in mock-infected mice ($p=0.002$). Pyramidal neurons displaying normal morphology in control tissue had faint cytoplasm that was roughly uniform in diameter around a clear nucleus with a prominent dark nucleolus (Fig. 17F).

The neuropil vacuolation in the cerebral cortex of moribund mice varied in severity between animals (Fig. 17A and G). Vacuoles also varied in size and prevalence throughout the cerebral cortex of individual animals, with clusters of severe vacuolation composed of various sized vacuoles occurring in a multifocal distribution throughout the cortex. The size of the neuropil vacuoles varied from the size of the irregular round vacuoles that were observed within the cytoplasm of the perikarya to the size of neuronal perikarya themselves, or slightly larger.

Pyramidal neurons in area CA1 of the hippocampus of CVS-infected moribund mice showed similar pathological findings to those found in pyramidal neurons of the cerebral cortex, but were not as frequent. Spherical vacuoles were observed in the cytoplasm and proximal dendrites of 21.7 ± 16.1% of pyramidal neurons in infected animals (Fig. 18A and C) vs. 0% in mock-infected animals ($p=0.41$). This comparison is not significant due to the lack of variance in values for the mock-infected group. Again, these vacuoles caused distention of the cytoplasm and distortion of the cell body. Pyramidal neurons in mock-infected mice did not show any signs of vacuolation and had faint cytoplasm which was approximately uniform in diameter around the nucleus (Fig. 18B and D).

Neuronal processes in the cerebellar white matter of CVS-infected mice displayed signs of swelling, including enlarged myelinated axons, creating the appearance of

vacuolation in this area (Fig. 18E). Since processes in white matter vary in diameter in controls (Fig. 18F), only the most severe abnormalities were apparent in infected tissues. Vacuoles were also present in the molecular layer.

G. Electron Microscopy

The predominant finding from electron microscopy studies of the cerebral cortex of moribund YFP mice was the presence of swollen mitochondria within the perikarya, dendrites and axons of pyramidal neurons (Fig. 19A and C; Fig. 20 A and C). The degree of swelling varied from increases in the size of the cristae spaces to empty matrices with a loss of cristae. However, some neurons displayed very little or no mitochondrial swelling, which indicates that these morphological changes are not due to fixation. Also, a few neurons that lacked mitochondrial swelling contained nucleocapsid material, indicating that these cells were still at an early stage in the injury process despite the moribund status of the animal. Swelling was also observed within the cisternae of the Golgi apparatus (Fig. 19A and C) in neurons with and without mitochondrial swelling, which suggests that swelling of the Golgi apparatus may precede mitochondrial swelling. Furthermore, pyramidal neurons in infected tissue appeared to have less well defined endoplasmic reticulum than control tissue. The swollen mitochondria likely correspond to the numerous round vacuoles observed within the perikarya and proximal dendrites of pyramidal neurons in toluidine blue stained sections of the cerebral cortex.

Axonal and dendritic beading may be the result of mitochondrial swelling in neuronal processes. Swollen mitochondria were found to co-localize with areas of increased diameter in neuronal processes (Fig. 20A). The severity of mitochondrial swelling was also greater in dendrites than axons, which correlates with observations

made using fluorescent microscopy that axonal beading was less severe than dendritic beading. In spite of these morphological alterations, numerous axondendritic synapses were present along the length of dendrites (Fig. 20C). Also, microtubules were observed throughout neuronal processes, while the presence of neurofilaments was more variable (Fig. 20C).

The neuropil vacuolation observed in toluidine blue stained tissue sections primarily represented severely distended neuronal processes and swollen nerve endings. Ultrastructurally, many of these neuropil vacuoles were found to contain mitochondria and microtubule debris. Furthermore, some of the vacuoles also contained synaptic vesicles or synaptic densities (Fig 20E), confirming a neuronal origin. In some cases, however, the vacuoles were devoid of any residual material. As such, we cannot exclude the possibility that some of the neuropil vacuoles may represent swollen astrocytes, particularly vacuoles surrounding blood vessels.

Despite the abnormal changes in organelle structure, cortical pyramidal neurons did not display features of major neuronal degeneration (Fig. 19A). There was no evidence of swelling of the cell body or degeneration of the plasma or nuclear membranes. Nuclei were clear and contained prominent nucleoli which did not display chromatin condensations. There were also multiple synapses between axon terminals and the perikarya. The presence of nucleocapsid material in the cytoplasm of the majority of pyramidal neurons displaying mitochondrial swelling confirmed that they were infected (Fig. 19A).

CHAPTER 5: TABLES

Table 1. Rabies virus infection was evaluated in the midbrain, cerebral cortex and hippocampus (CA1 and CA3 regions) of mice inoculated in the right hindlimb footpad or intracerebrally and treated with either vehicle or ketamine twice daily on days 3 through 6 p.i. (n=4 in each treatment group on each day, except n=3 on day 5 in the intracerebrally inoculated ketamine-treated group). Slides stained for rabies virus antigen were blinded and the numbers of infected neurons were counted in three different fields with the most marked staining within the same brain region using high power (40x) objective. Counts are expressed as the mean score ± standard error of the mean. Treatment with vehicle or ketamine was compared using an unpaired t-test, and a p value < 0.05 was considered to be significant.

Brain Region	Vehicle	Ketamine	p value
Footpad Inoculation			
Day 3			
Midbrain	0 ± 0	0.3 ± 0.3	0.42
Cerebral cortex	0 ± 0	0 ± 0	1.00
Hippocampal subfield CA1	0 ± 0	0 ± 0	1.00
Hippocampal subfield CA3	0 ± 0	0 ± 0	1.00
Day 4			
Midbrain	2.4 ± 1.8	1.0 ± 0.7	0.49
Cerebral cortex	0.3 ± 0.3	0 ± 0	0.42
Hippocampal subfield CA1	0 ± 0	0 ± 0	1.00
Hippocampal subfield CA3	0 ± 0	0 ± 0	1.00
Day 5			
Midbrain	18.2 ± 1.7	6.8 ± 6.5	0.14
Cerebral cortex	26.0 ± 15.5	5.2 ± 4.0	0.24
Hippocampal subfield CA1	0 ± 0	0 ± 0	1.00
Hippocampal subfield CA3	0 ± 0	0 ± 0	1.00
Day 6			
Midbrain	29.6 ± 4.3	29.1 ± 5.0	0.94
Cerebral cortex	58.7 ± 9.3	53.9 ± 4.6	0.66
Hippocampal subfield CA1	1.9 ± 1.6	0.6 ± 0.6	0.46
Hippocampal subfield CA3	6.4 ± 4.0	6.2 ± 5.8	0.97
Intracerebral Inoculation			
Day 3			
Midbrain	0.5 ± 0.3	0.5 ± 0.3	1.00
Cerebral cortex	0.8 ± 0.4	0.5 ± 0.3	0.79
Hippocampal subfield CA1	1.3 ± 0.7	5.3 ± 1.1	0.13
Hippocampal subfield CA3	6.2 ± 3.2	19.7 ± 4.7	0.24
Day 5			
Midbrain	27.0 ± 3.0	25.3 ± 2.6	0.80
Cerebral cortex	76.3 ± 10.5	76.4 ± 11.6	0.99
Hippocampal subfield CA1	33.6 ± 6.0	32.9 ± 7.3	0.97
Hippocampal subfield CA3	52.8 ± 4.1	68.6 ± 10.5	0.40

Table 2. Morphological changes of apoptosis were evaluated in neurons in the cerebral cortex and hippocampus (CA1 and CA3 regions) of mice inoculated intracerebrally with CVS and treated with either vehicle or ketamine twice daily (40x objective). A semiquantitative evaluation of the severity of apoptotic changes was performed on day 3 p.i. (no changes observed) or day 5 p.i (vehicle, n=4; ketamine, n=3) or once mice were moribund (vehicle, n=3; ketamine, n=6) with the following scheme: 0, no significant changes; 1, mild changes; 2, moderate changes; 3, severe changes; and 4, very severe changes and/or neuronal loss. The identity of all slides was masked during scoring in order to prevent bias in the evaluation. Rating scale scores are expressed as the mean score ± standard error of the mean. Treatment with vehicle or ketamine was compared using the Mann Whitney test, and a p value < 0.05 was considered to be significant.

Brain Region	*Ketamine*	*Vehicle*	*p-value*
Day 5			
Cerebral cortex	0.3 ± 0.3	0 ± 0	0.42
Hippocampal subfield CA1	0.7 ± 0.3	0.8 ± 0.5	1.00
Hippocampal subfield CA3	2.0 ± 1.0	1.3 ± 0.8	0.65
Moribund			
Cerebral cortex	1.3 ± 0.2	1.0 ± 0	0.40
Hippocampal subfield CA1	2.8 ± 0.5	4.0 ± 0	0.25
Hippocampal subfield CA3	3.7 ± 0.3	4.0 ± 0	0.65

CHAPTER 6: FIGURES

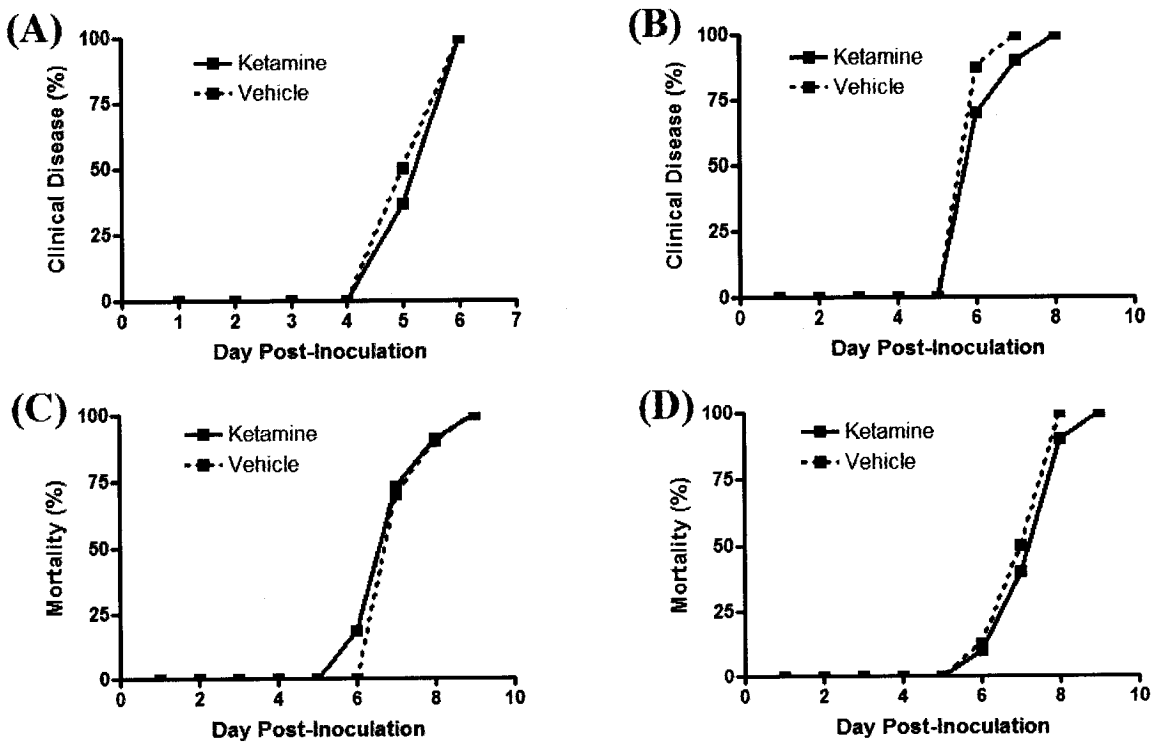

Figure 1. Kaplan-Meier curves of the cumulative neurological signs of disease (A, B) and cumulative mortality (C, D) in mice inoculated in the right hindlimb footpad (A, C) or intracerebrally (B, D) with CVS and treated twice daily with vehicle (dashed) or ketamine (solid). Vehicle treatment (A and C, n=10; B and D, n=8) and ketamine treatment (A and C, n=11; B and D, n=10) groups were compared using log rank tests, which indicated that there was no difference in the mortality rate between treatment groups (A, p=0.54; B, p=0.30; C, p=0.53; D, p=0.50).

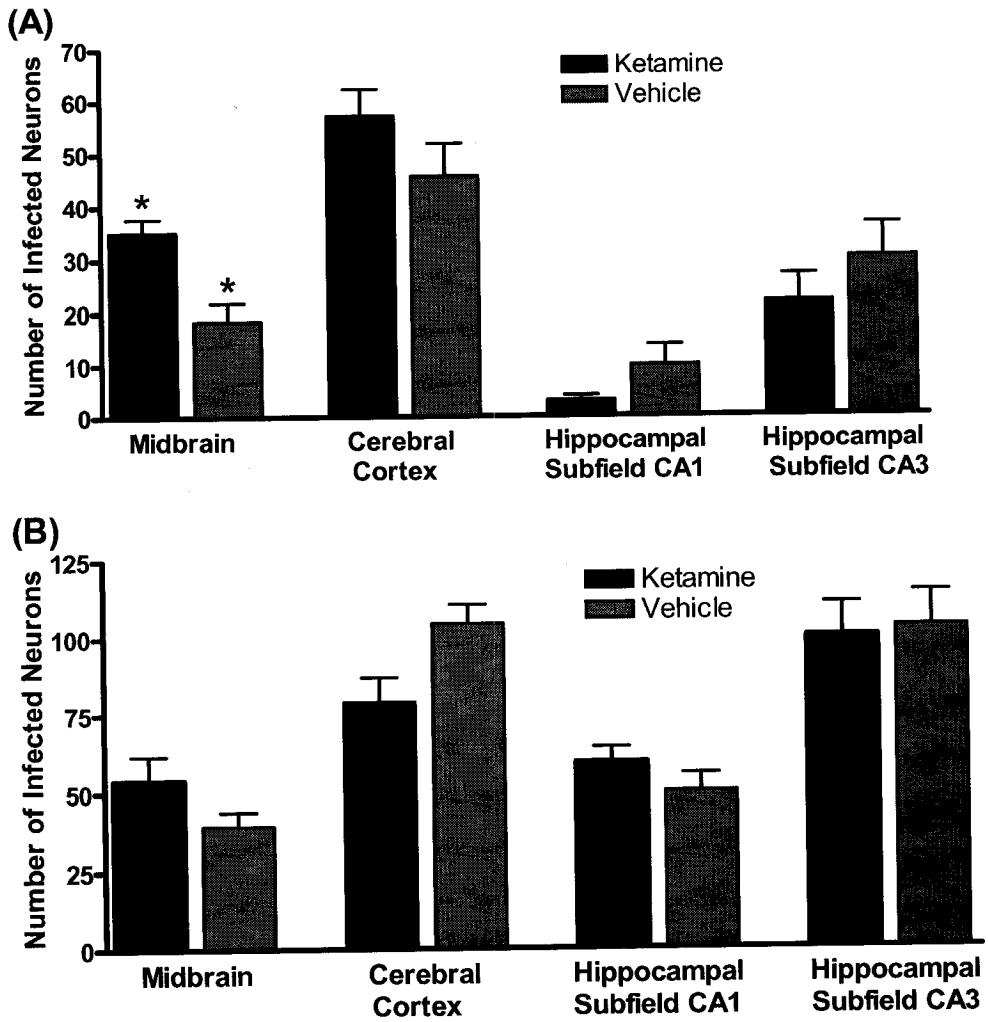

Figure 2. Counts of the number of infected neurons in various brain regions of moribund mice after right hindlimb footpad (A) and intracerebral (B) inoculation of CVS and twice daily treatment with vehicle (shaded) or ketamine (solid). Slides stained for rabies virus antigen were blinded and the numbers of infected neurons were counted in three different fields of the same brain region using high power (40x) objective in areas with the most marked staining. Vehicle treatment (A, n=8; B, n=3) and ketamine treatment (A, n=11; B, n=6) groups were compared using an unpaired *t*-test (* represents statistical significance at a confidence level of 95%) and the error bars represent the standard error of the mean.

Figure 3. Rabies virus antigen in the cerebral cortex (A, B), CA3 region of the hippocampus (C, D) and midbrain tegmentum (E, F) in vehicle- (A, C, E) and ketamine- (B, D, F) treated moribund mice infected with CVS via hindlimb footpad inoculation showing a similar distribution, although more infected neurons were present in the midbrain with ketamine treatment. Cresyl violet staining of the CA1 region of the hippocampus from moribund mice infected with CVS intracerebrally that received vehicle (G) and ketamine (H) showing many apoptotic neurons with condensations of nuclear chromatin. Magnification: A and B, x85; C and D, x260; E and F, x45; G and H, x525

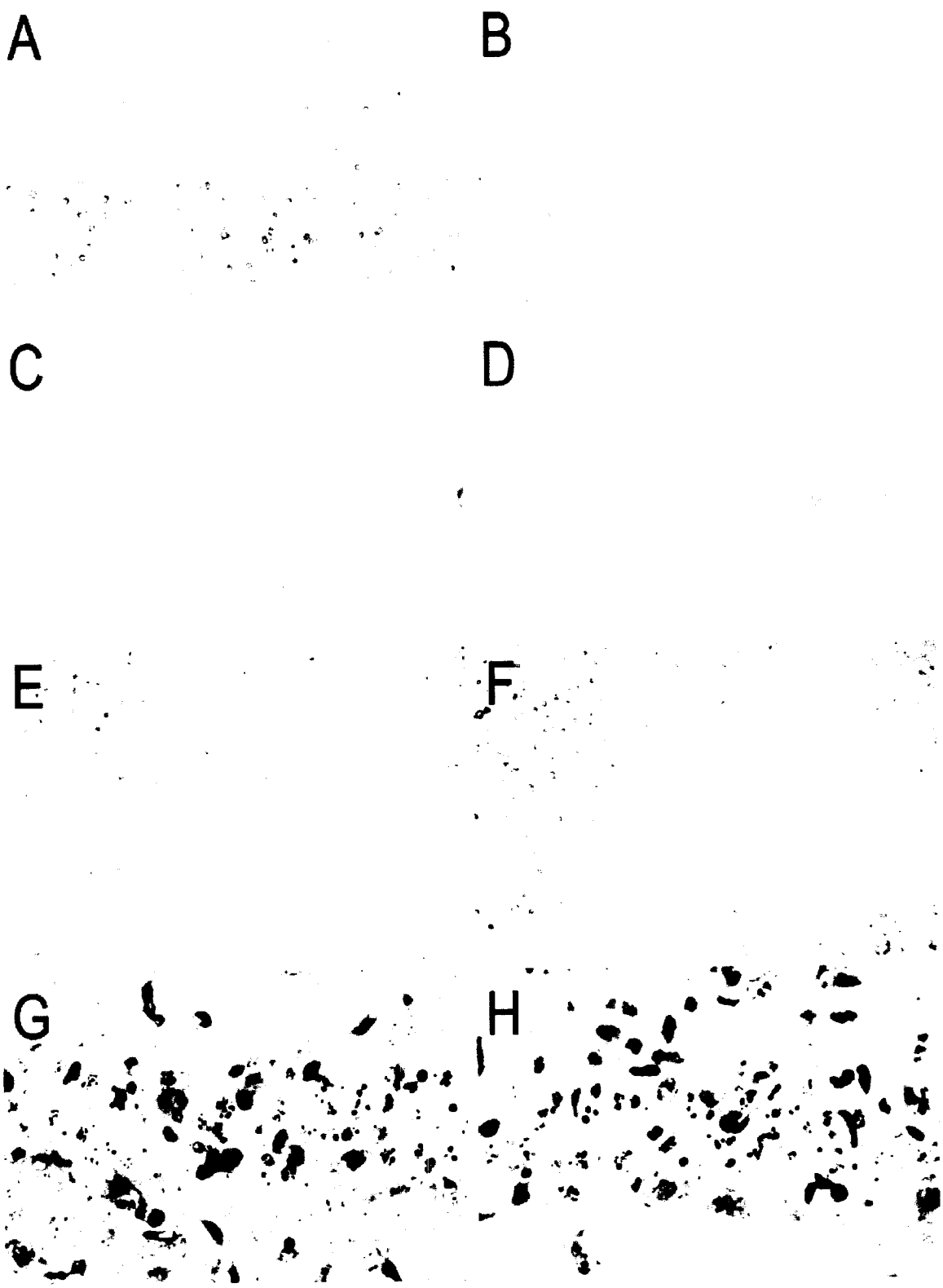
A
B
C
D
E
F
G
H

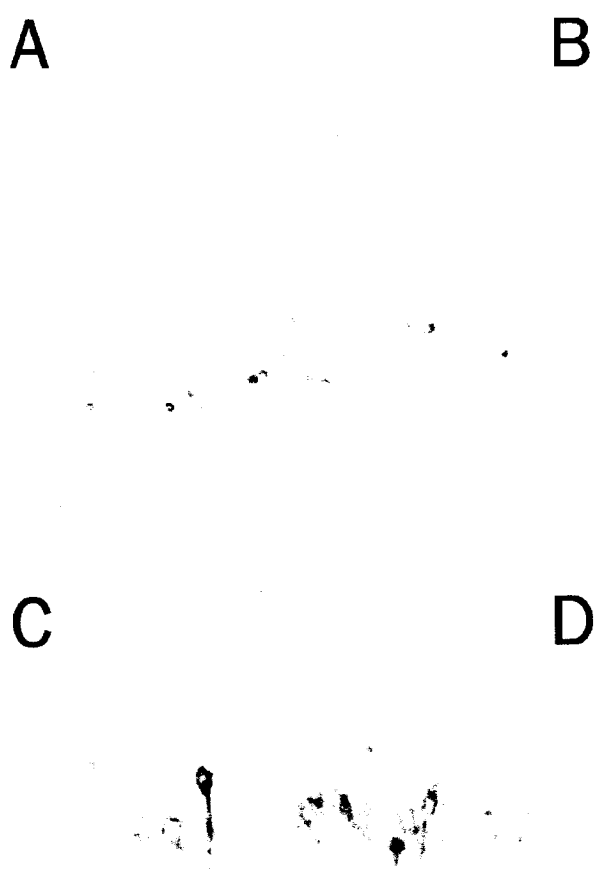

Figure 4. Rabies virus antigen in the cerebral cortex (A, B) and area CA1 of the hippocampus (C, D) in moribund YFP mice infected with CVS (A, C) or mock-infected YFP mice (B, D). Widespread infection was observed in the perikarya and dendritic processes of pyramidal neurons throughout both of these regions in infected mice. Control tissues showed low background staining. Magnification: A and B, 100x; C and D, 200x

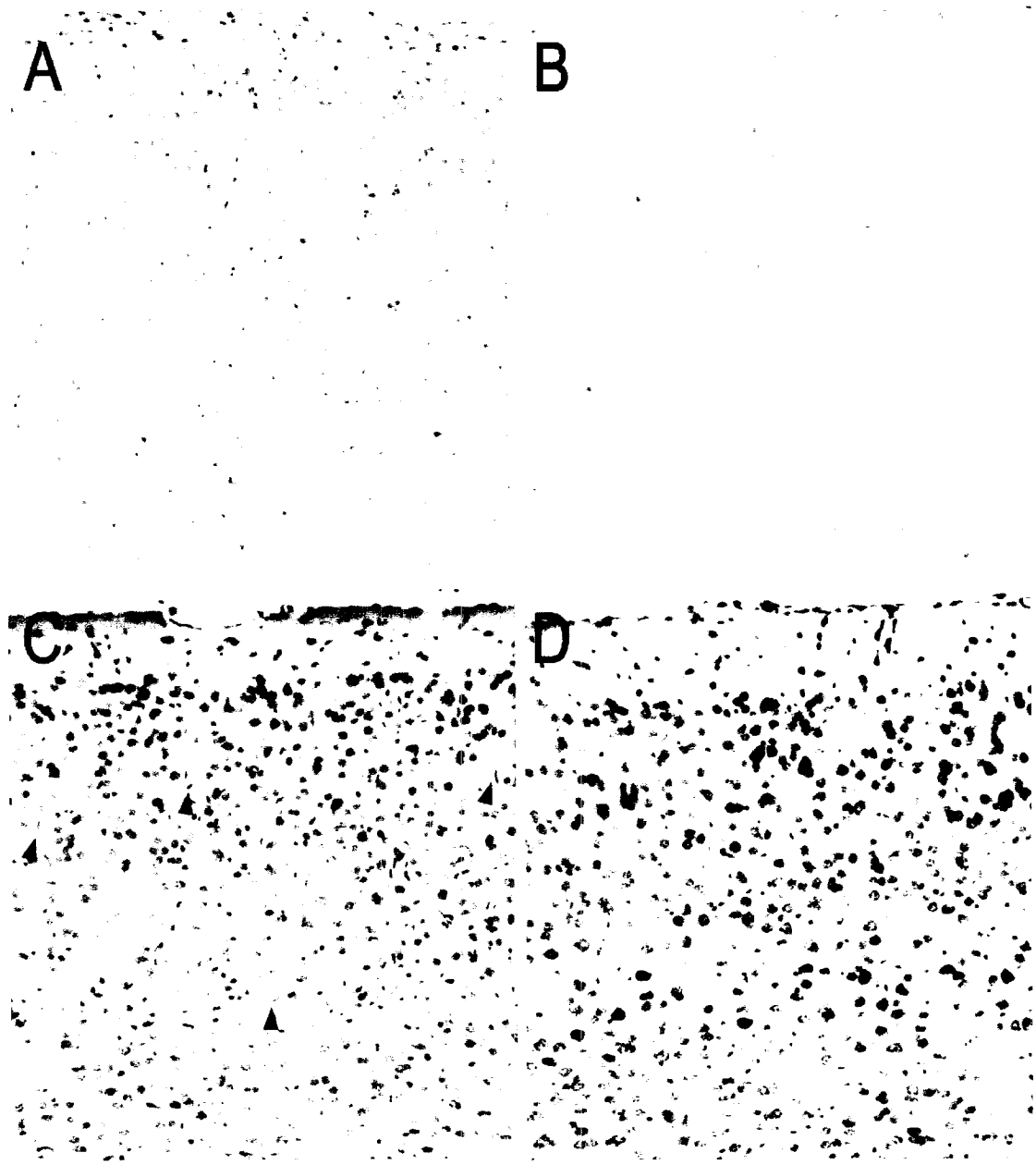

Figure 5. Hematoxylin and eosin (A, B) and cresyl violet (C, D) staining of the cerebral cortex in moribund YFP mice inoculated with CVS (A, C) or mock-infected YFP mice (B, D). Activated microglia were present throughout the cerebral cortex, particularly surrounding blood vessels, in infected mice (arrowheads). Magnification: 126x

Figure 6. Hematoxylin and eosin (A, B) and cresyl violet (C, D) staining of area CA1 of the hippocampus in moribund YFP mice inoculated with CVS (A, C) or mock-infected YFP mice (B, D). Activated microglia are present throughout the hippocampus in infected mice (arrowheads). Magnification: 215x

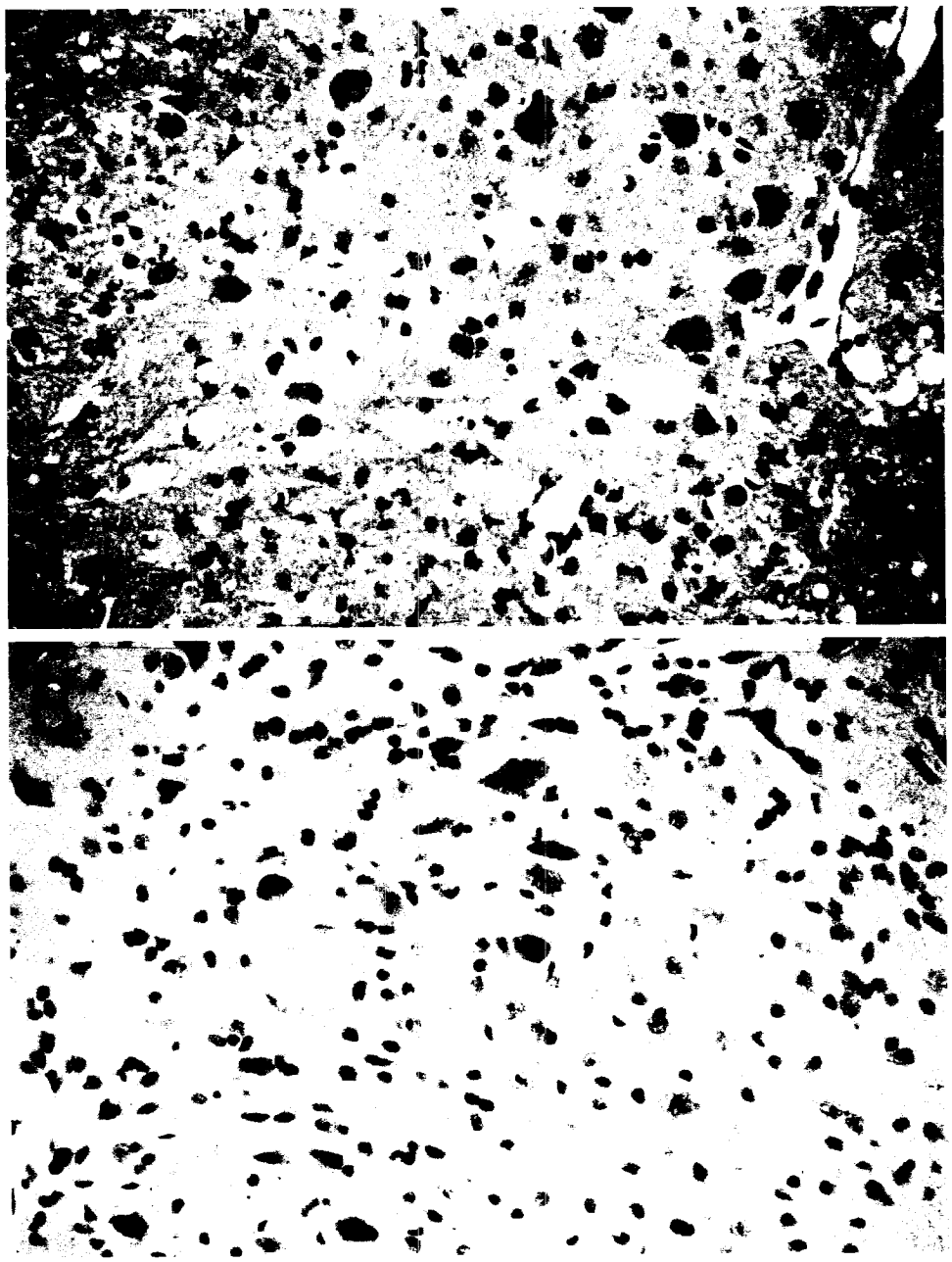

Figure 7. Hematoxylin and eosin staining of the cerebellum of moribund YFP mice inoculated with CVS (A) or mock-infected YFP mice (B). Extensive vacuolation is evident in the deep cerebellar white matter in infected mice (A). Magnification: 300x

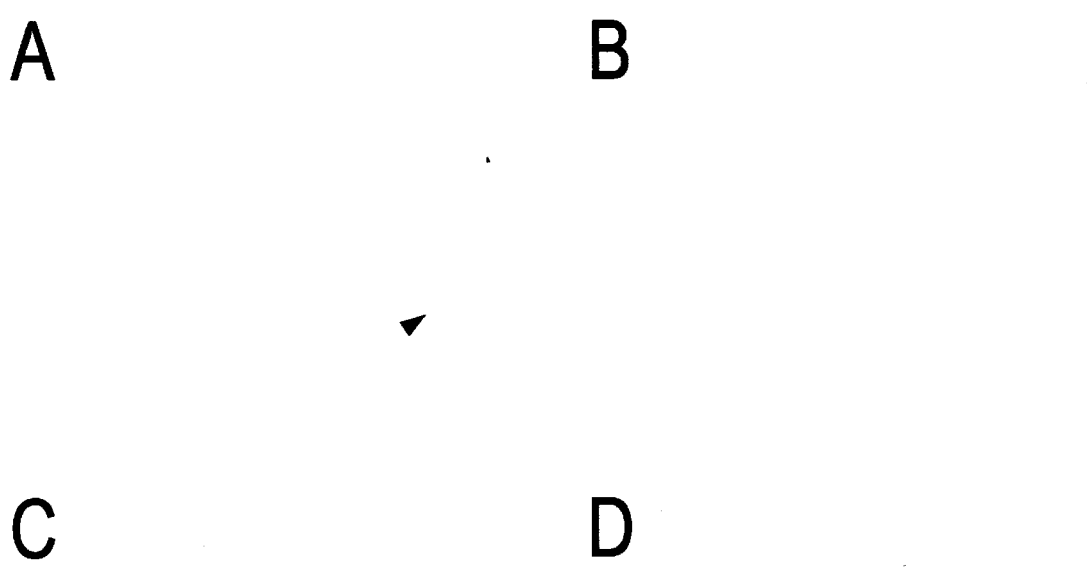

Figure 8. Caspase-3 immunostaining in the cerebral cortex (A, B) and area CA1 of the hippocampus (C, D) in moribund YFP mice inoculated with CVS (A, C) or mock-infected YFP mice (B, D). A rare caspase-positive cell was observed in the cerebral cortex of CVS-infected mice (arrowhead). Low background staining was observed in the hippocampus of infected mice (C) and in mock-infected mice (B, D). Magnification: A and B, 113x; C and D, 227x

Figure 9. TUNEL staining in the cerebral cortex (A, B, C) and area CA1 of the hippocampus (D, E, F) in moribund YFP mice infected with CVS (A, C, D, F) or mock-infected YFP mice (B, E). Positive controls (C, F), pre-treated with DNAase, showed widespread staining, while infected mice only showed staining in a few scattered cells, which were likely inflammatory cells, in the cerebral cortex (A, arrowheads). The hippocampus of infected mice (D) and tissue from mock-infected mice (B, E) showed low background staining. Magnification: A, B and C, 109x; D, E and F, 218x

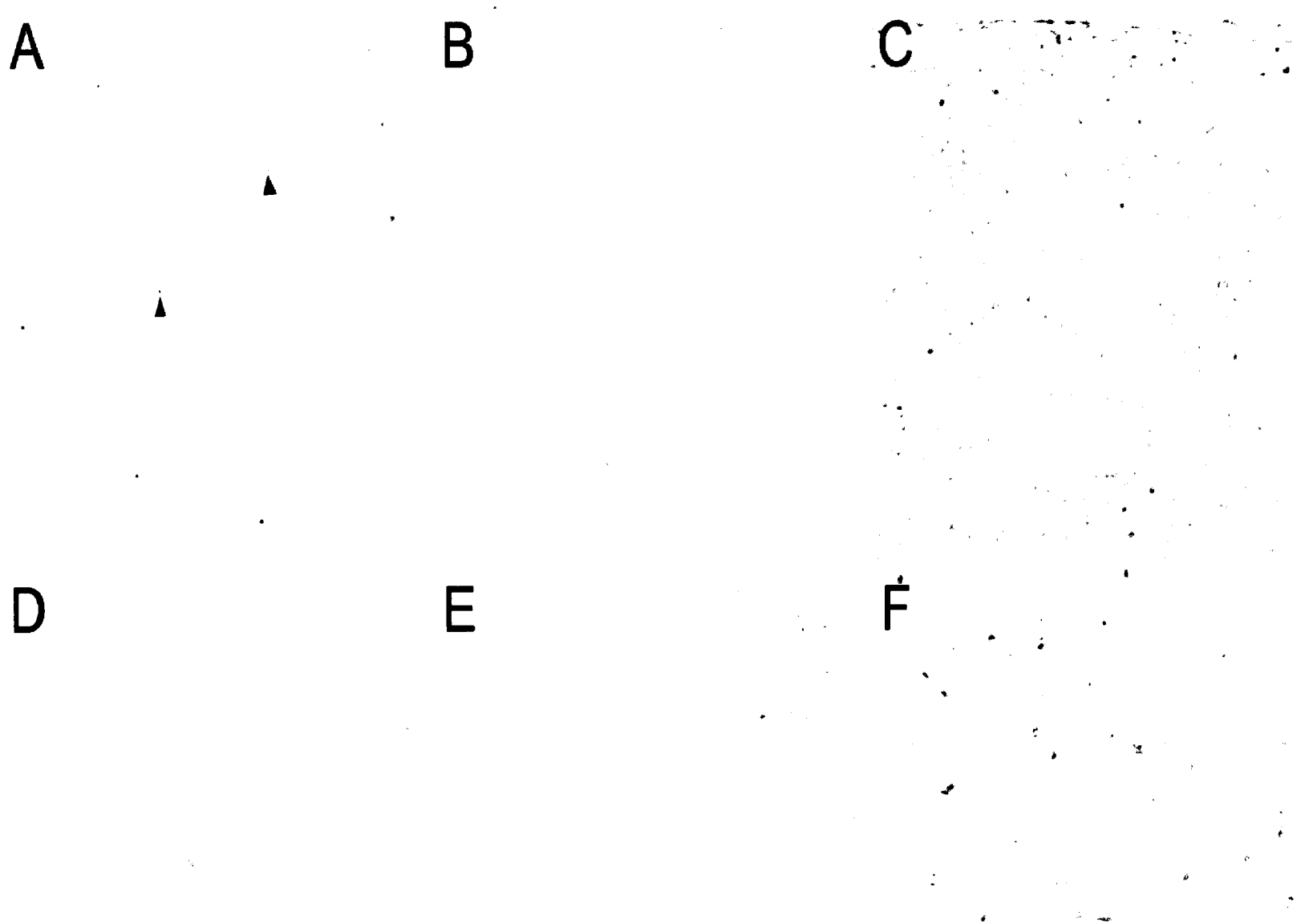
A
B
C
D
E
F

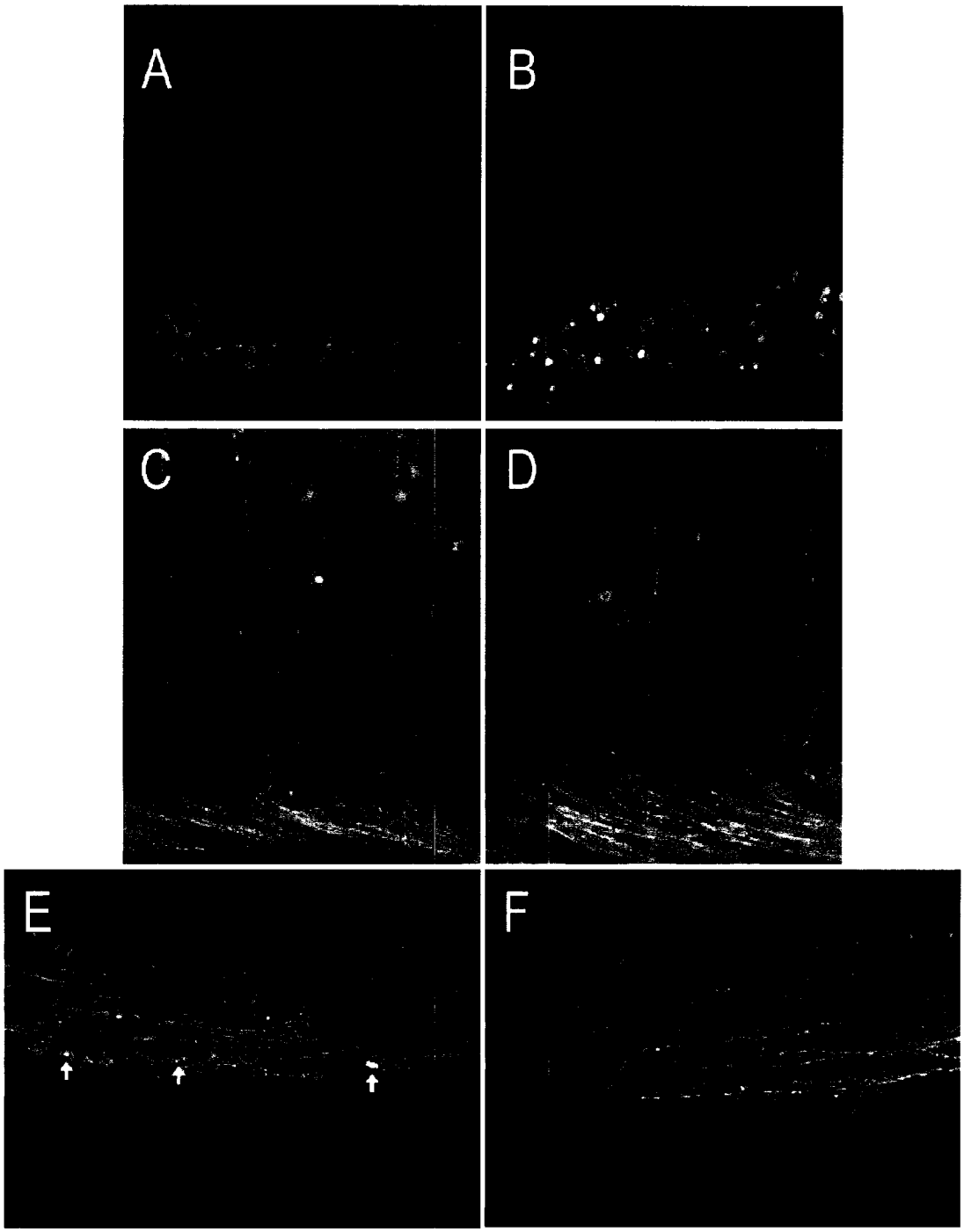

Figure 10. Minor morphological abnormalities in neuronal processes of CVS-infected YFP mice displaying hindlimb paralysis. Dendrites (A, B) and axons (C, D) in the cerebral cortex of infected (A, C) and mock-infected (B, D) mice were morphologically very similar. Mossy fibers in the cerebellar commissure of CVS-infected mice show minor beading (E, arrows) compared to mock-infected tissues (F). Magnification: A, B, E and F, 85x; C and D, 205x

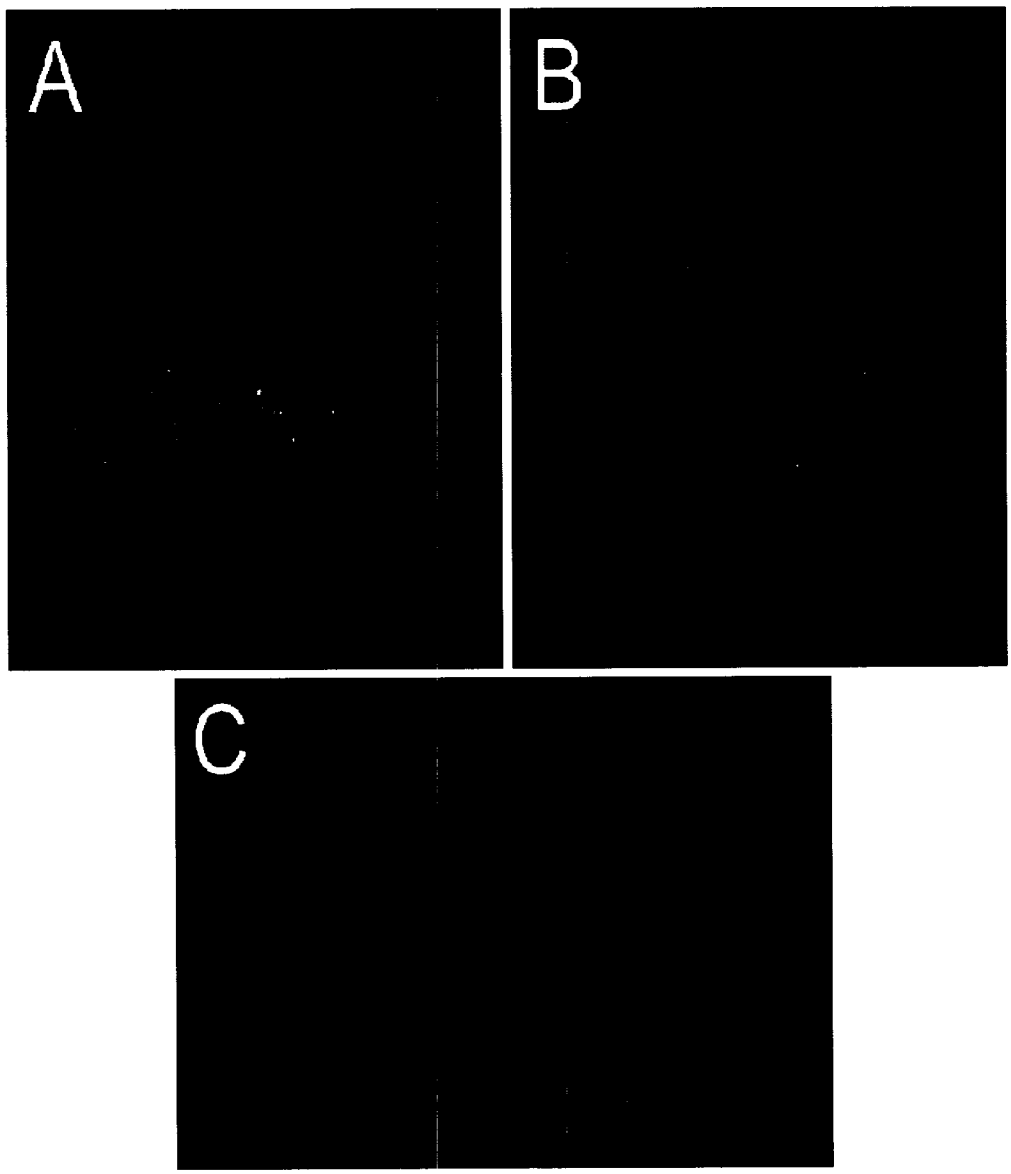

Figure 11. Fluorescent rabies virus antigen staining in the cerebral cortex (A, B) and hippocampus (C) of CVS-infected YFP mice that displayed right hindlimb paralysis (A) or were moribund (B, C). Rabies virus antigen was present throughout the cerebral cortex of mice with right hindlimb paralysis. In moribund animals, rabies virus antigen was widespread in the cerebral cortex and hippocampus. Magnification: 60x

Figure 12. Morphological abnormalities in layer V pyramidal neurons in the cerebral cortex of moribund YFP mice inoculated with CVS (A, C, E, G). Beading and fragmentation is observed in a minority of dendrites (A, C, E), while axons are less severely beaded but more involved (G) in infected mice. There are no abnormalities in the dendrites (B, D, F) or axons (H) of mock-infected mice. Axons in mock-infected mice are slightly varicose (H), which is characteristic of these fibers. Magnification: A and B, 85x; C, D, G and H 205x; E and F, 340x

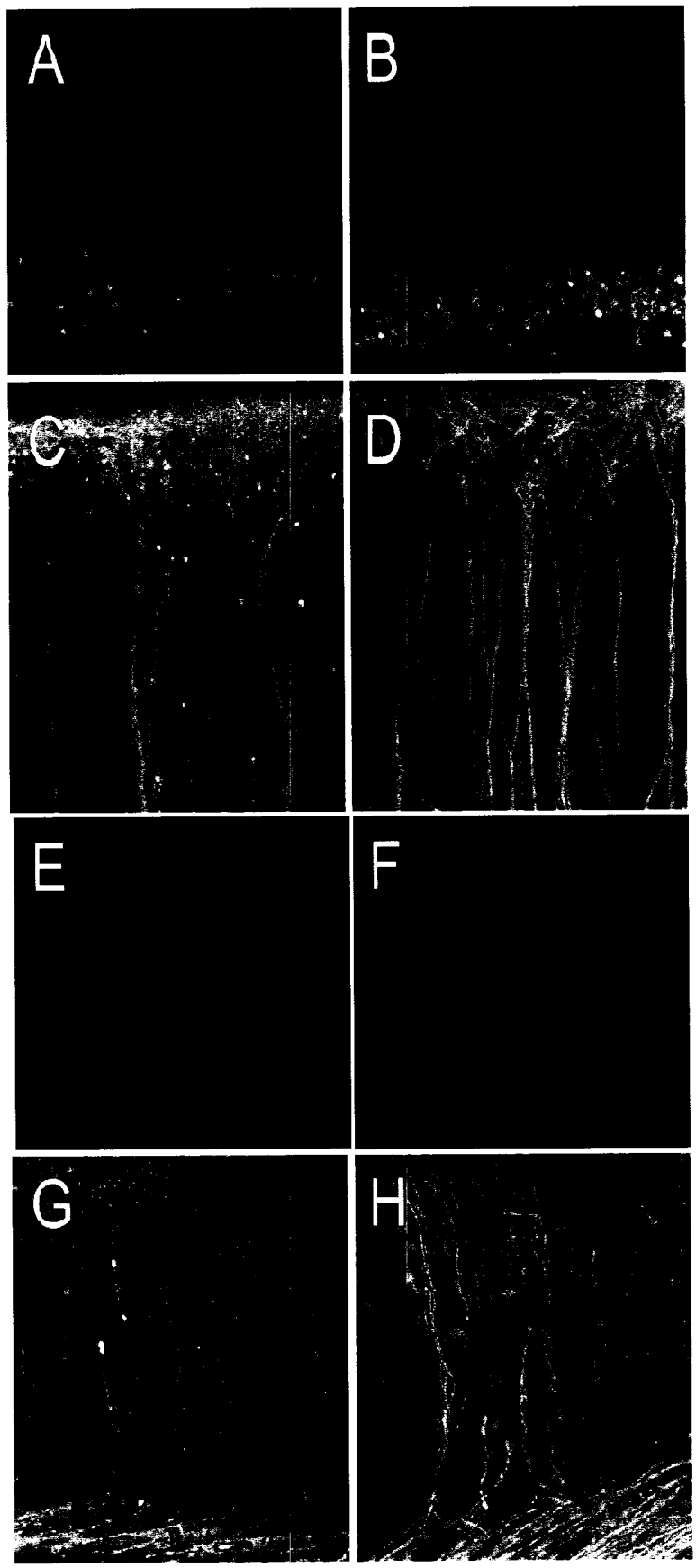
A
B
C
D
E
F
G
H

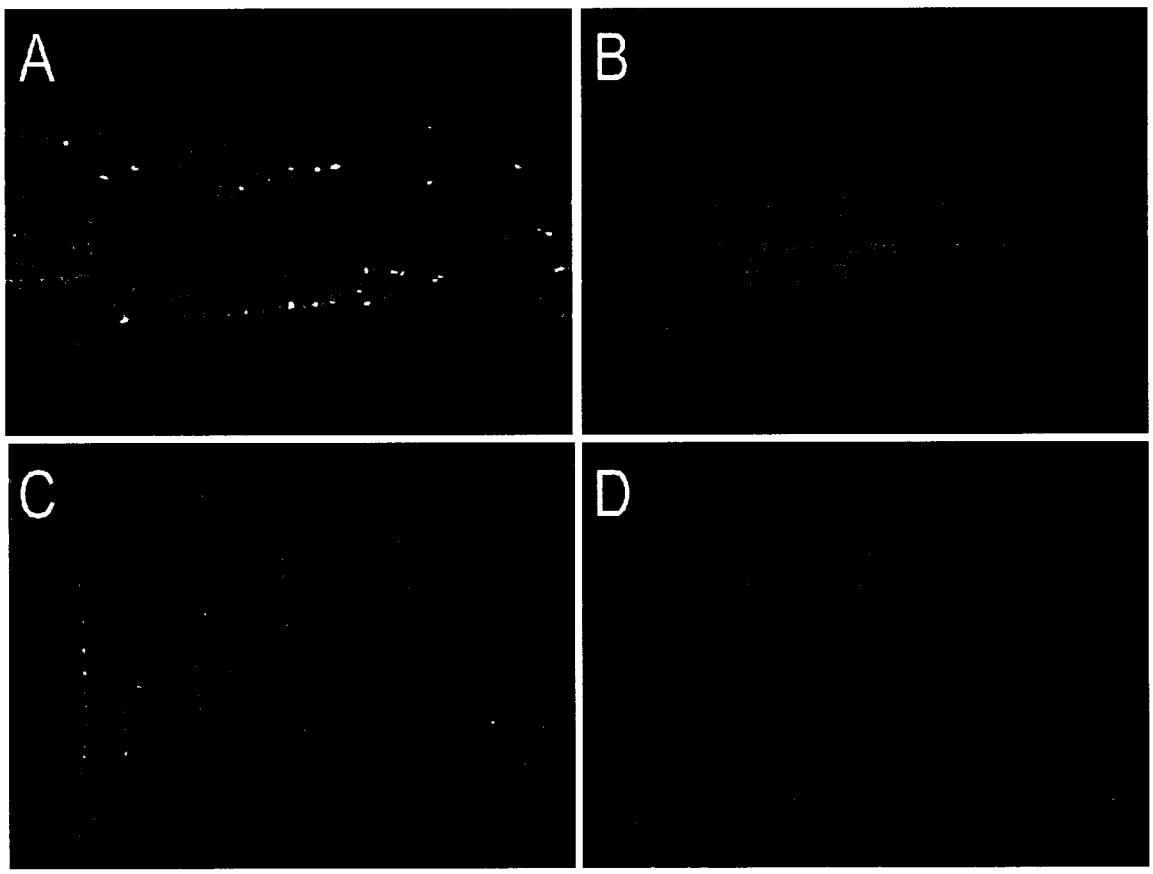

Figure 13. Morphological abnormalities in the cerebellar mossy fibers of moribund YFP mice inoculated in the hindlimb footpad with CVS. Mossy fibers in the cerebellar commissure show severe beading and fragmentation (A), while mossy fibers entering the granular layer show signs of beading (C). No abnormalities were observed in mock-infected mice (B, D). Magnification: 85x

Figure 14. Morphological abnormalities in YFP-positive axonal processes in the brainstem of moribund YFP mice inoculated with CVS in the right hindlimb footpad. (A, C) Central tracts traveling rostral-caudally displayed distended processes (arrows) and may have some degree of axonal loss. (E) Processes in the inferior cerebellar peduncles were also beaded (arrows). (B, D, F) Tracts in mock-infected mice did not display any abnormalities. (G) The pontine nuclei did not display fluorescent perikarya, indicating that it was not an important source of the fluorescent cerebellar mossy fibers. (H) The neurons in the vestibular nuclei of moribund transgenic mice expressed YFP and fibers originating from this nucleus traveled into the cerebellum and displayed beading. Magnification: A, B, E, F, G and H 60x; C and D, 155x

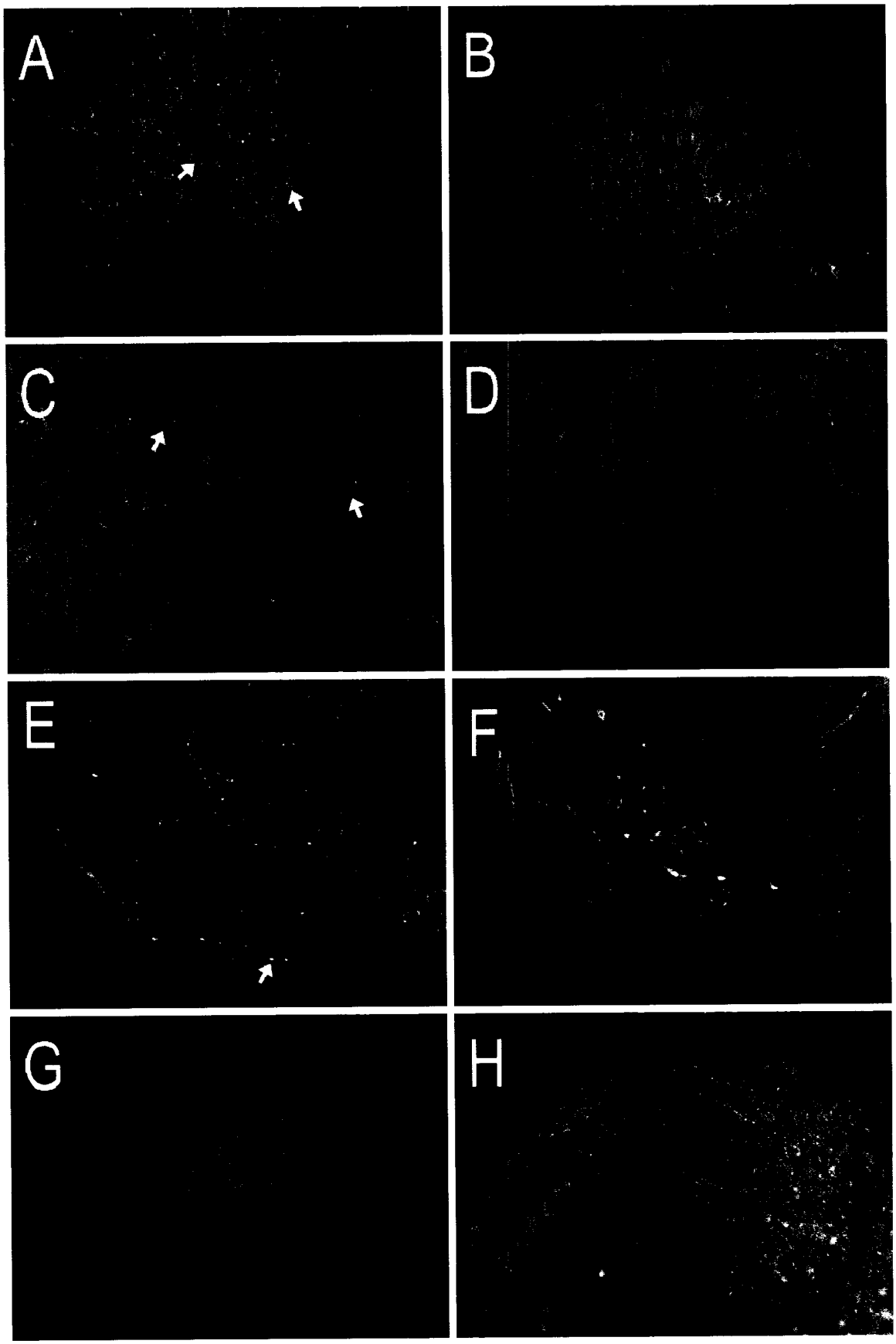
A
B
C
D
E
F
G
H

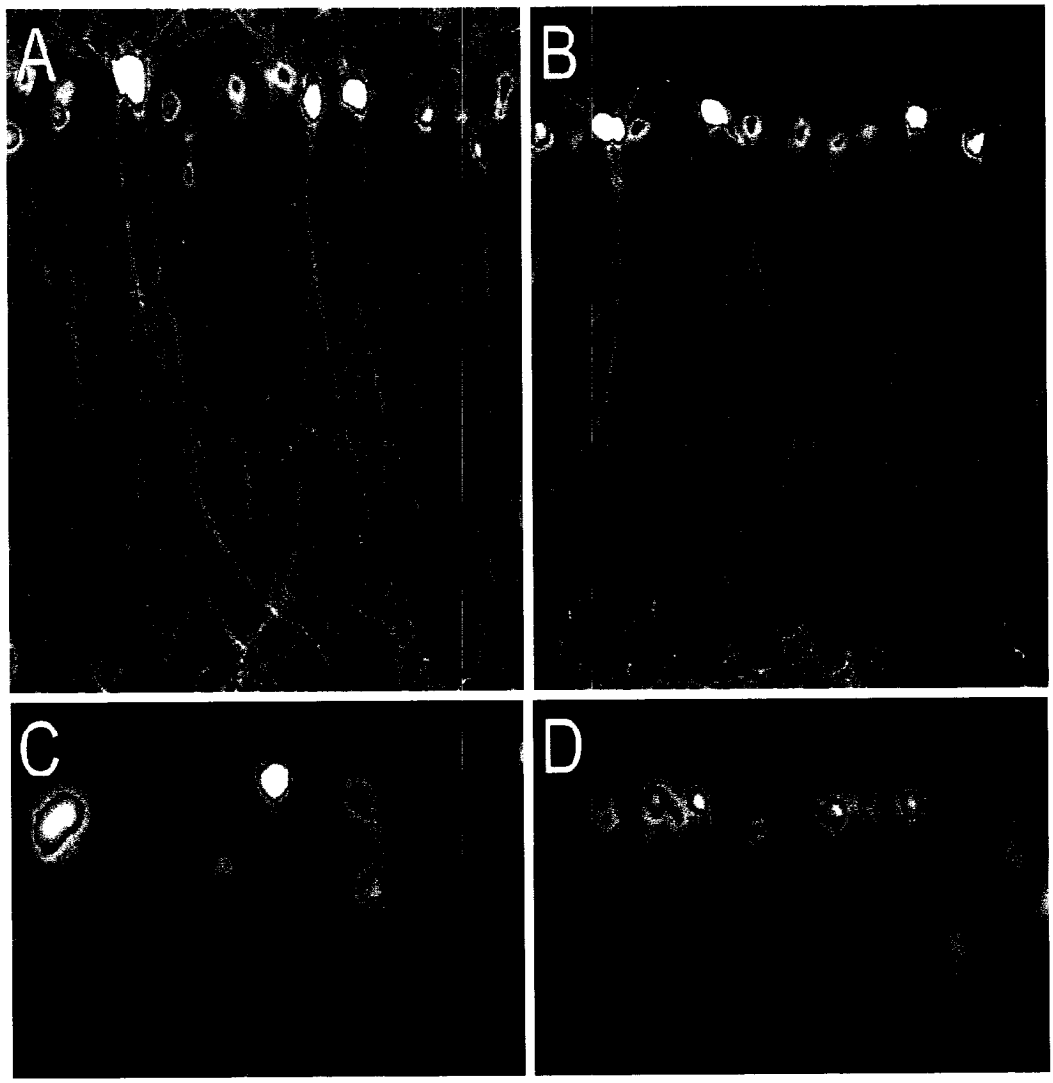

Figure 15. Rare morphological abnormalities in area CA1 of the hippocampus in moribund YFP mice inoculated with CVS in the right hindlimb footpad. The hippocampi of infected (A) and mock-infected (B) mice were morphologically very similar. Shrunken and degenerating perikarya were rarely observed (C, D). Magnification: A and B, 205x; C and D, 340x

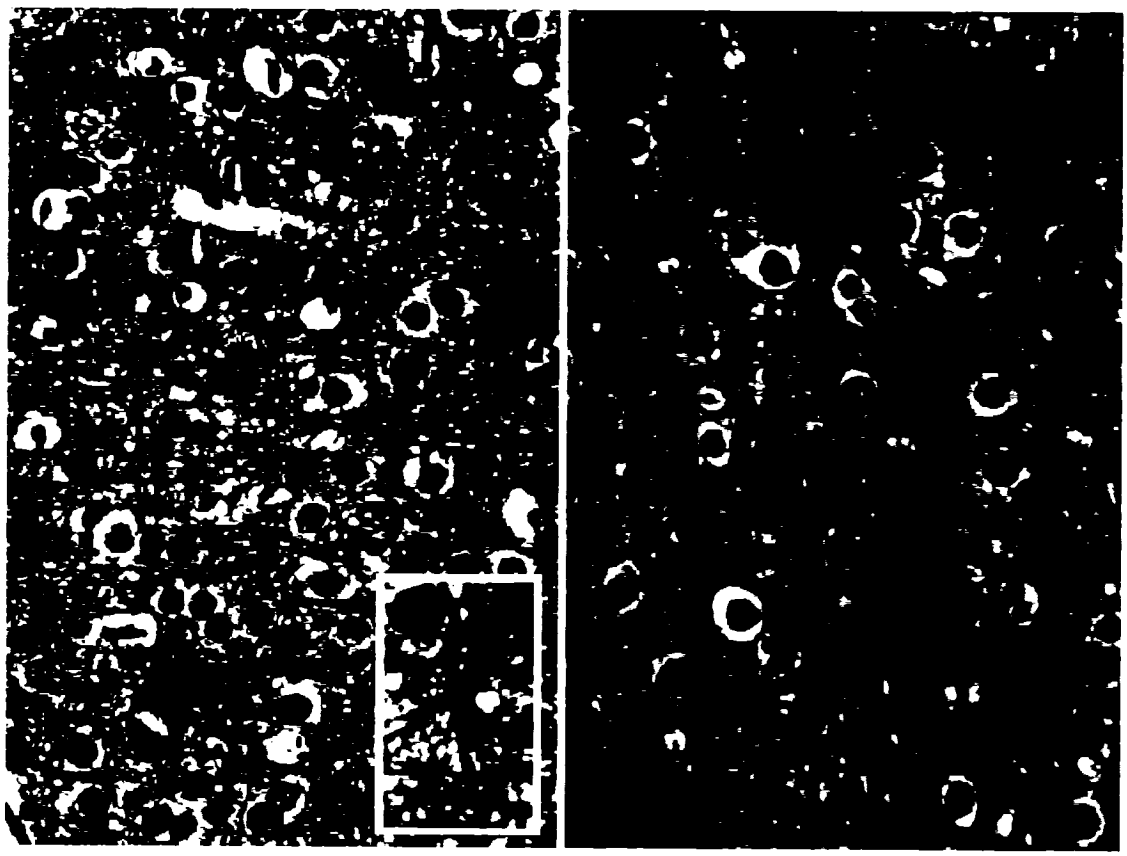

Figure 16. Silver staining of axons in the cerebral cortex of moribund YFP mice peripherally inoculated with CVS (A) or mock-infected YFP mice (B). Rare axons in tissues from moribund animals displayed evidence of minor beading and undulating courses as they traveled from the neuron cell bodies to the deep white matter of the cortex (arrow indicates magnified area in inset). Magnification: A and B, 414x; inset, 920x

Figure 17. Toluidine blue staining in the cerebral cortex of moribund YFP mice infected with CVS (A, C, D, E) or mock-infected YFP mice (B, F). Numerous round vacuoles were observed within the perikarya and proximal dendrites of many layer V pyramidal neurons in infected mice (C, D, E), but were rare in mock-infected mice (F). Vacuolation was also observed throughout the neuropil in infected mice (A, G), which was not observed in control tissues (B). Magnification: A and B, 484x; C, D, E and F, 1412x; G, 1051x

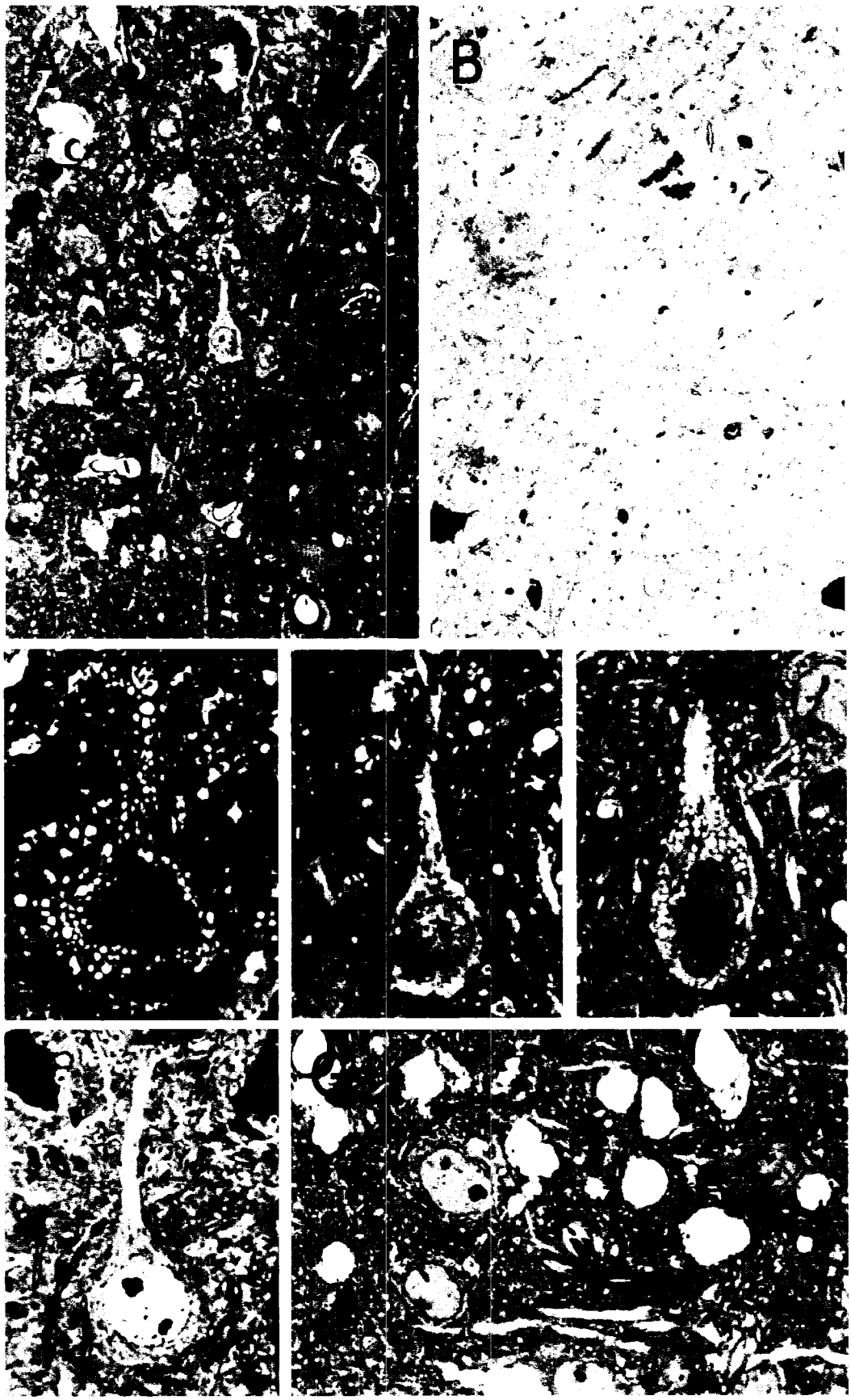
C
B

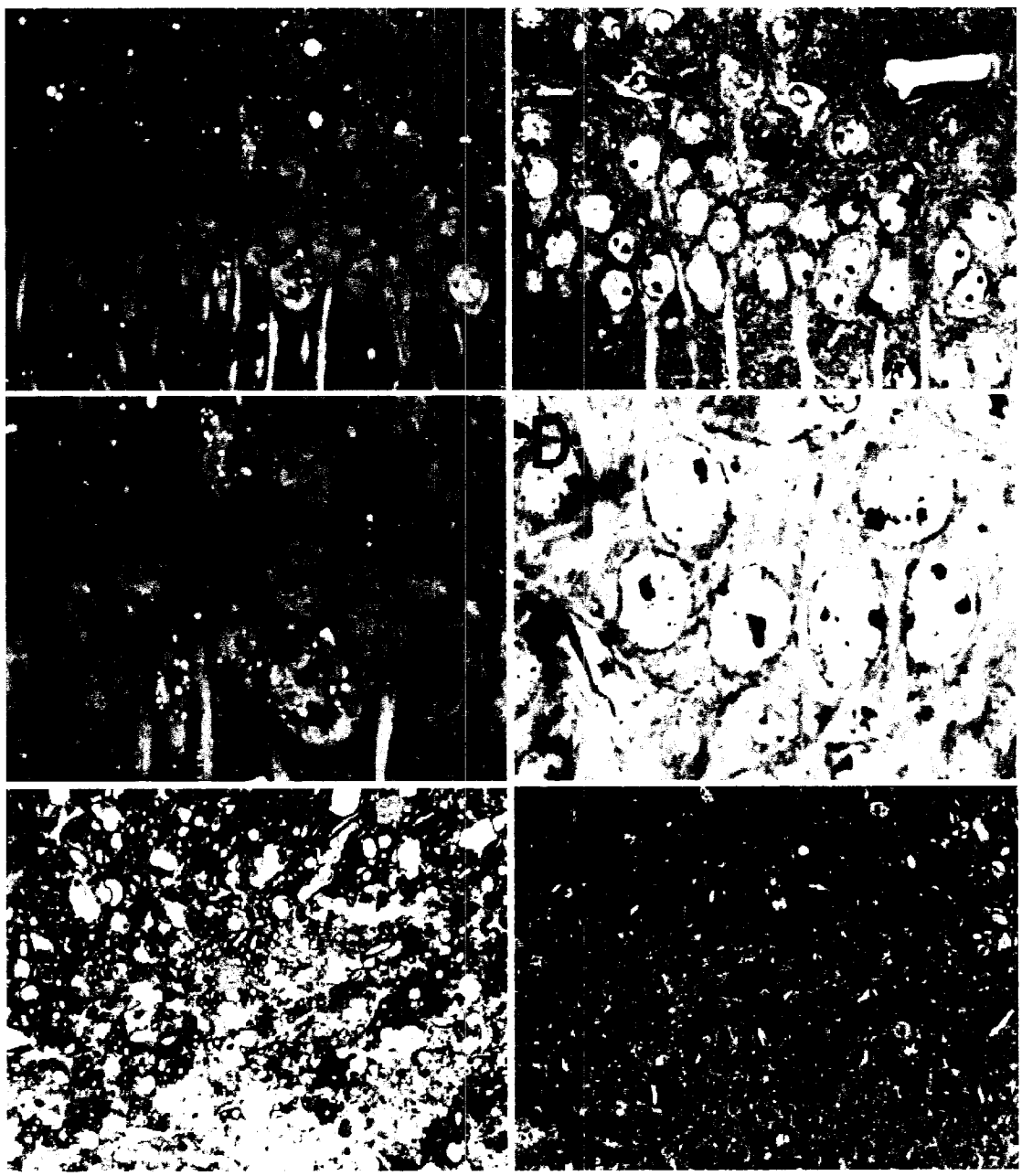

Figure 18. Toluidine blue staining in area CA1 of the hippocampus (A, B, C, D) and the cerebellum (E, F) of moribund YFP mice infected with CVS (A, C, E) or mock-infected YFP mice (B, D, F). Numerous round vacuoles were observed in the perikarya and proximal dendrites in infected mice (A, C), but were not observed in mock-infected mice (B, D). Vacuolation was observed within the cerebellar white matter of infected mice (E) which was not present in mock-infected mice (F). Magnification: A and B, 531x; C and D, 1327x; E and F, 403x

Figure 19. Electron micrographs of pyramidal neurons in the cerebral cortex of CVS-infected moribund YFP mice (A and C) and mock-infected YFP mice (B). (A) Swollen mitochondria (solid arrows) are present throughout the cytoplasm of the perikarya and proximal dendrite of a pyramidal neuron in infected tissue, while the nuclear membrane and plasma membrane remain intact. Virus nucleocapsid material (arrowhead) and swollen Golgi apparatus (open arrow) are also observed in the cytoplasm of the perikarya. (C) A magnified view of the boxed area in (A) shows swollen mitochondria (solid arrow) and swollen Golgi apparatus (open arrow) in the cytoplasm of an infected pyramidal neuron. (B) Mitochondria (solid arrows) in mock-infected tissues are elongated and the cristae are compact.

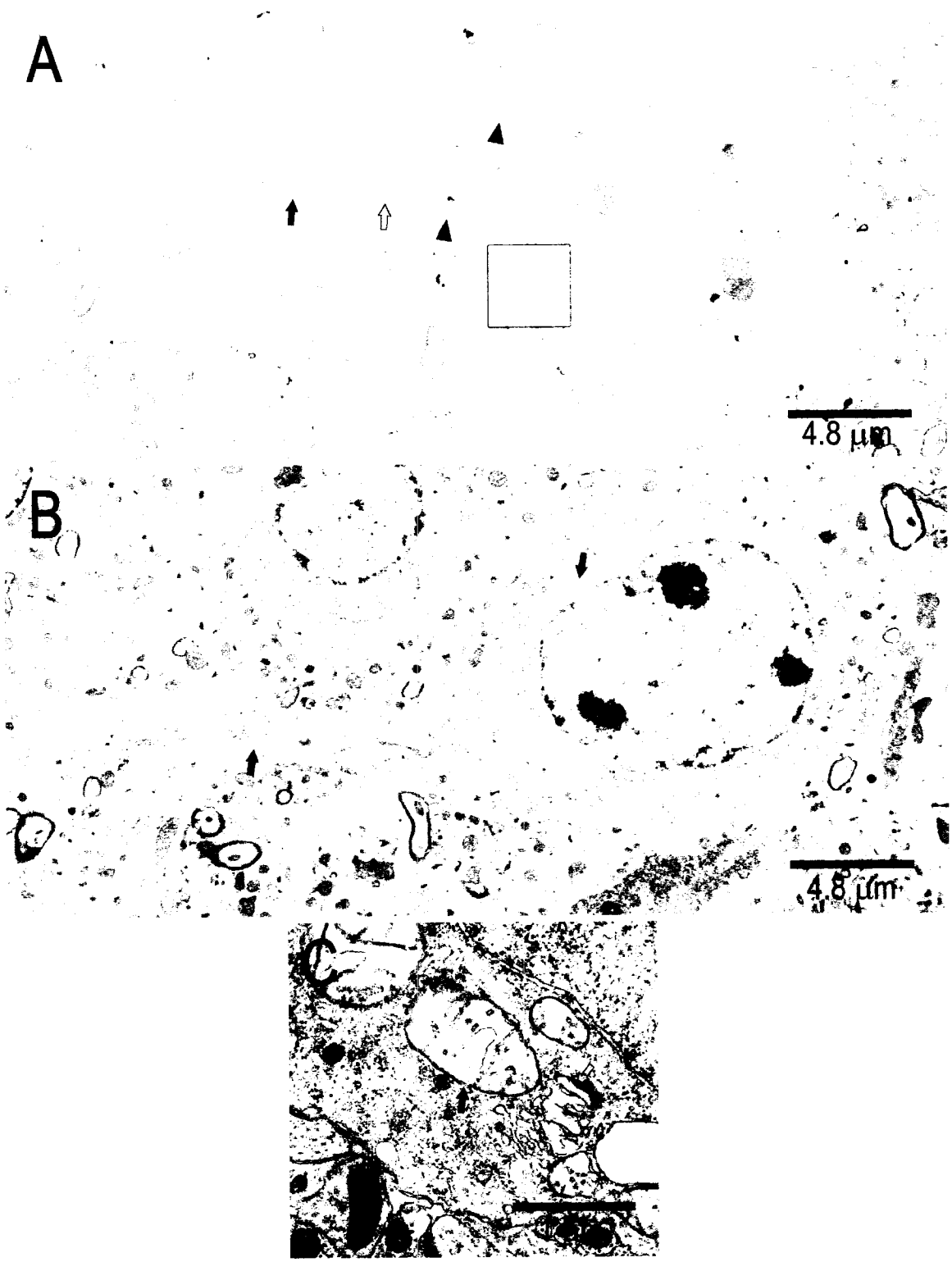
A
4.8 µm
B
4.8 µm

Figure 20. Electron micrographs of the cerebral cortex of CVS-infected moribund YFP mice (A, C, E) and mock-infected YFP mice (B and D). (A) Axons of pyramidal neurons contained swollen mitochondria (solid arrow) in infected tissues, which corresponded with areas of beading. (C) Dendrites in infected tissues also contained swollen mitochondria (solid arrow), while the microtubules and an axodendritic synapse (arrowhead) were morphologically normal. (E) Vacuoles in the neuropil of infected tissues contained synaptic vesicles (arrowheads), indicating that they are neuronal in origin and represent pre-synaptic nerve endings (inset is a magnified view of the synaptic vesicles indicated by the lower left arrowhead). (B, D) Mitochondria (arrows) in mock-infected tissues mitochondria are elongated and the cristae are compact.

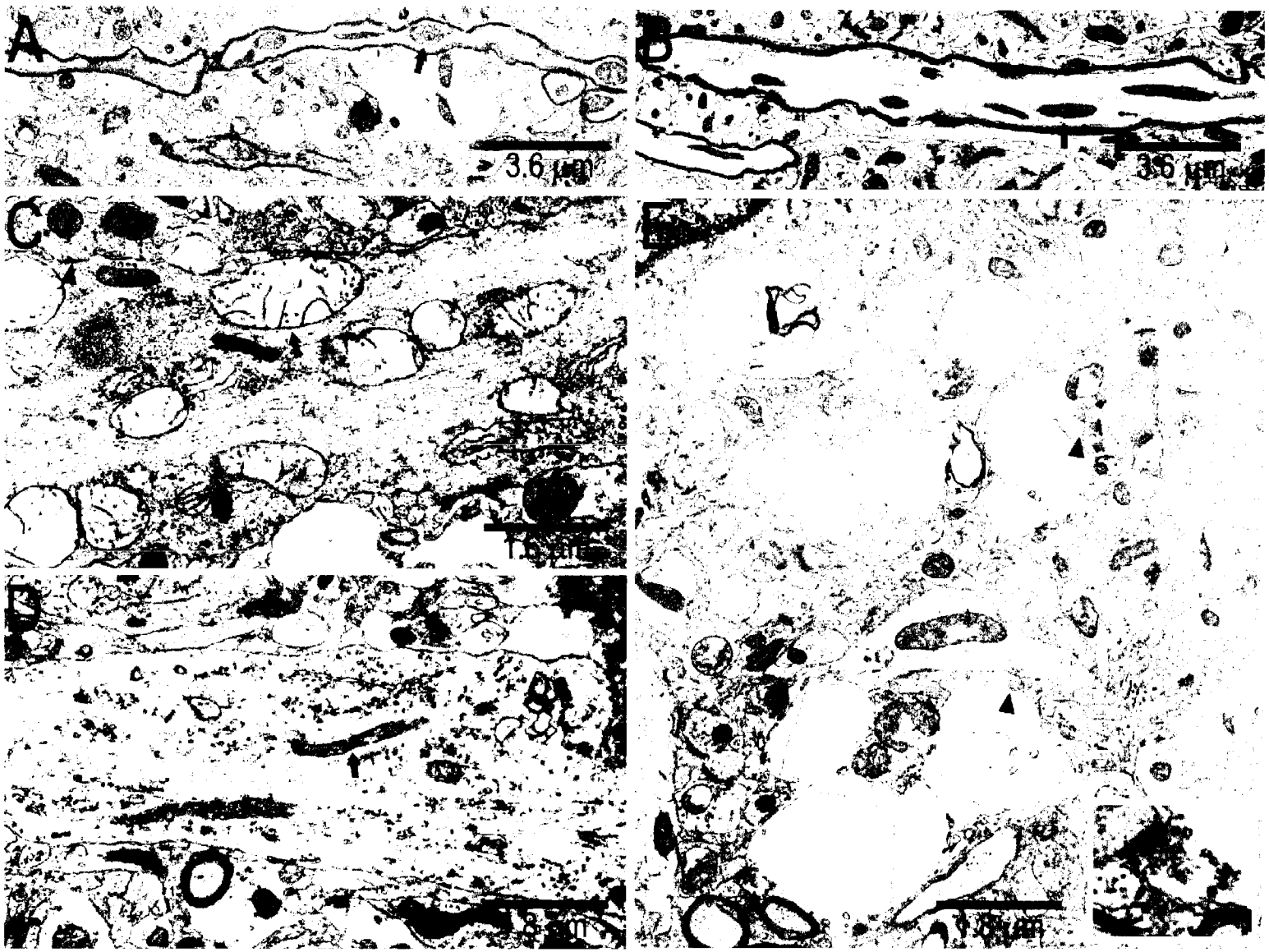
A
3.6 μm
B
3.6 μm
C
1.6 μm
D
8 μm
E
1.6 μm

CHAPTER 7: DISCUSSION

The rabies virus is a highly neurotropic virus which causes acute infection of the CNS for which there is no effective antiviral therapy in humans. Despite its lethality, only mild histopathological lesions are found under natural conditions, suggesting that neuronal dysfunction, rather than neuronal death, is responsible for the clinical features and fatal outcome (Jackson, 2002; Fu and Jackson, 2005). However, mechanisms of neuronal dysfunction are still not understood (Fu and Jackson, 2005). A number of viral-induced diseases of the CNS were shown to be a result of the action of excitatory amino acids on the N-methyl-D-aspartate acid (NMDA) receptor, or the pathological process known as excitotoxicity (Nath *et al.*, 2000; Nargi-Aizenman *et al.*, 2001; Darman *et al.*, 2004). Studies with rat cortical neurons and with a rat model suggested the possibility that the noncompetitive NMDA receptor antagonists ketamine and MK-801 might be effective therapeutic agents for human rabies (Lockhart *et al.*, 1991; Tsiang *et al.*, 1991b; Lockhart *et al.*, 1992) and that ketamine inhibits viral RNA genome transcription (Lockhart *et al.*, 1992). A recent human rabies survivor also received therapy with ketamine, amongst other drugs (Willoughby *et al.*, 2005). Consequently, we have examined the hypothesis that excitotoxicity may play an important role in the pathogenesis of rabies. In the present study, we evaluated the effects of ketamine and examined morphological changes with an emphasis on the structural integrity of neuronal processes in experimental rabies in mice in order to assess whether excitotoxicity could be the basis for neuronal dysfunction in rabies virus infection.

The administration of ketamine (60mg/kg every 12 h intraperitoneally) to CVS-infected ICR mice did not result in reduced mortality or the amelioration of clinical neurological disease compared to the administration of vehicle. There was also no

reduction in the number of infected neurons in various brain regions over the time course of infection in ketamine-treated mice. These findings contrast with those reported by Lockhart and colleagues (1991) who demonstrated, using more qualitative methods of analysis than in the current study, that the same dosage of ketamine inhibited viral spread after stereotaxic inoculation of rats with CVS. Ketamine is metabolized in the liver by the cytochrome P-450 proteins 1A, 2B, 2E1 and 3A (Chan *et al.*, 2005) and mice have more 2E1 and 1A activity than rats (Nakajima *et al.*, 1993). Although mice metabolize ketamine more rapidly than rats (Olson and Renchko, 1988), and therefore require higher doses of ketamine to achieve anesthesia (100 mg/kg vs. 40-60 mg/kg intraperitoneally), a lesser dose of ketamine (20mg/kg) than that used in the present study has been shown to be neuroprotective in a mouse model of and epilepsy (Guler *et al.*, 2005). Similarly, a 2, 5 or 10 mg/kg dose of ketamine was found to suppress endotoxin-induced NF-κB expression, which plays a primary role in ischemic and traumatic brain injury (Sakai *et al.*, 2000). Also, the antiviral dosage of ketamine used by Lockhart and colleagues (1991) could be much higher than the neuroprotective dosage. It is highly unlikely that there is a species-specific difference in the therapeutic effect of ketamine. Furthermore, virus entry using footpad inoculation better evaluates viral spread through the neuroaxis than by stereotaxic inoculation, and provides a more comprehensive analysis of the therapeutic efficacy of ketamine, or lack thereof.

CVS infection via the intracerebral route of inoculation is associated with widespread neuronal apoptosis (Jackson and Rossiter, 1997). Neuronal apoptosis is also produced by the action of high concentrations of glutamate or its analogues on the ionotropic glutamate receptors, particularly the NMDA receptor (Koh *et al.*, 1990; Park *et al.*, 1996; Hasbani *et al.*, 1998). However, therapy with ketamine did not reduce the

severity of apoptotic changes in the brains of intracerebrally inoculated ICR mice, nor did it provide beneficial effects clinically or histopathologically. In *in vitro* studies, we also found that ketamine, as well as MK-801, did not provide any significant neuroprotective effect in CVS-infected primary cultures of cortical and hippocampal neurons, which also demonstrated morphological features of apoptosis (Weli *et al.*, 2006).

Peripheral inoculation with CVS, on the other hand, is characterized by inflammation of the brain and spinal cord without prominent neuronal apoptosis (Reid and Jackson, 2001; Jackson, 2003). YFP mice inoculated in the hindlimb footpad with CVS displayed inflammatory changes throughout the cerebral cortex, hippocampus and cerebellum, including inflammation of the leptomeninges and parenchyma and perivascular cuffing. Despite widespread infection, as demonstrated by rabies virus antigen staining, terminal deoxynucleotidyl transferase mediated dUTP nick end labeling (TUNEL) staining, which is a marker for apoptosis that is not entirely specific, was minimal in the cerebral cortex and hippocampus of moribund mice. TUNEL staining also labeled a few non-neuronal cells, which were likely inflammatory cells. Staining for activated caspase-3, which is a downstream executioner of the apoptosis pathway, was rare in the cerebral cortex and was not observed in area CA1 of the hippocampus. Overall, there was no well defined pathology in the brains of CVS-infected YFP mice under light microscopy despite the advanced neurological disease.

However, when tissue from CVS-infected YFP mice was examined using fluorescent microscopy, previously unrecognized morphological abnormalities were observed in neuronal processes of the cerebral cortex, cerebellum and brainstem. These structural changes ranged in severity from interspersed swellings on intact processes, also known as beading, to severely distended sections of neuronal processes which lacked

apparent physical connections between the residual swollen pieces (fragmentation). Neuronal perikarya, however, were largely unaffected with only rare shrunken cell bodies observed in the cerebral cortex and area CA1 of the hippocampus of moribund animals. These morphological findings appeared relatively late in the time course of infection. Only minor beading was observed in the cerebellar commissure at an early time point (6 days p.i.) despite widespread infection of the cerebellum and cerebral cortex at this time, which suggests that these changes do not function to limit the spread of rabies through the neuroaxis. These structural alterations resemble dendrotoxicity, which is a typical feature of excitotoxicity. Dendrotoxicity is characterized by the formation of large swellings or "beads," which are separated from each other by thin dendritic segments, with preservation of the neuronal cell body (Olivia *et al.*, 2002). Beading is believed to result from the intracellular movement of sodium and chloride, but not calcium, through NMDA receptors (Hasbani *et al.*, 1998; Al-Noorie and Swann, 2000).

Despite the morphological similarities between the beading observed in rabies virus infection and the beading resulting from excitotoxicity, there are important differences in the localization of these structural abnormalities which suggest that excitotoxicity is likely not the cause of beading in rabies virus infected neurons. In particular, the hippocampus is among the brain regions most vulnerable to excitotoxic injury (Olney *et al.*, 1979). In contrast, our study demonstrated relatively few structural abnormalities in the hippocampus of CVS-infected YFP mice, although this brain region is prominently infected in rabies. It is known that the hippocampus is infected relatively late in comparison to the rest of the brain following peripheral inoculation of CVS (Jackson and Reimer, 1989), which could potentially account for the minimal morphological changes observed within this structure. However, rabies virus antigen

staining, although sparse, was observed in the hippocampus at an early time point when mice displayed hindlimb paralysis (day 6 p.i.), and extensive staining was observed in moribund animals (days 9 through 12 p.i.).

The presence of axonal beading in rabies virus infected tissues is another distinguishing feature that differs from dendrotoxicity. In CVS-infected YFP mice, beading was observed in axons of layer V pyramidal neurons in the cerebral cortex, ascending and descending axonal tracts within the brainstem and in the cerebellar mossy fibers. Excitotoxicity, on the other hand, is characterized by selective dendritic injury, which is one of the earliest signs of excitotoxic injury and occurs in a number of neurological disease and neurodegenerative disorders (Park et al., 1996; Hasbani *et al.*, 1998; Vanicky *et al.*, 1998). The vulnerability of dendrites, and not axons, to excitotoxic injury can be explained by the predominantly somatodendritic distribution of glutamate receptors. Axons are, however, capable of undergoing beading concurrently with dendritic beading when the route of sodium entry is through voltage-sensitive channels, rather than receptor-operated channels (Hasbani *et al.*, 1998). Simultaneous beading in dendrites and axons has also been observed following the cortical superfusion of cats with ouabain, a Na^+/K^+ ATPase inhibitor which causes an intracellular build-up of sodium (Lowe, 1978). The expression of Na^+/K^+ ATPase has been shown to decrease in mice infected with the B2C strain of rabies virus resulting in an increase in intracellular sodium (Dhingra *et al.*, 2007). These findings indicate that sodium entry is sufficient to initiate the process of beading and suggest that the initiation of varicosity formation is not necessarily unique to glutamate-gated channels. Furthermore, axonal beading does not appear to result from the activation of ionotropic glutamate receptors.

The mechanism underlying beading also appears to differ between excitotoxicity

and rabies virus infection. In cortical neurons exposed to NMDA, the resulting varicosities were found to contain fragmented microtubules (Emory and Lucas, 1995), and similar findings were also observed in beaded dendrites from human cortical biopsies (Purpura *et al.*, 1982). In addition, transient NMDA exposure of hippocampal slices is associated with the loss of microtubule associated protein 2 (MAP-2) from dendrites (Hoskison and Shuttleworth, 2006; Hoskison *et al.*, 2007), which can be reduced by treatment with glutamate release inhibitors (Springer *et al.*, 1997). The outcome of cytoskeletal degradation is the accumulation of organelles and cytoplasm in regions where microtubule loss is sufficient to interrupt cytoplasmic transport, resulting in the formation of varicosities (Emery and Lucas, 1995). In this study, ultrastructural examination of the cytoskeleton revealed intact microtubules throughout the length of beaded neuronal processes in the cerebral cortex, while the presence of neurofilaments was more variable. Silver staining, which stains cytoskeletal elements, also revealed the preservation of cytoskeletal architecture in the cerebral cortex, hippocampus and cerebellum of moribund YFP mice. Similarly, Lockhart and colleagues (1992) found no gross alterations in cytoskeletal organization following infection of rat cortical neurons. Changes in the shape of neuronal processes may represent localized disturbances of volume regulation mediated solely by the entry of ions and water (Hasbani *et al.*, 1998). Although Li *et al.* (2005) reported a loss of MAP-2 staining in the processes of primary neurons infected with the pathogenic N2C strain of the rabies virus, their findings described destruction and disorganization of neuronal processes as opposed to beading. They also used a different virus strain that is more pathogenic than the one used in the present study, which could potentially explain the differences in cytoskeletal integrity. Also, these findings were observed *in vitro* as opposed to *in vivo*.

Based on the fluorescent microscopy studies, it appears that rabies virus infection selectively alters the morphology of neuronal processes following peripheral inoculation, while neuronal perikarya remain relatively unchanged. However, more detailed morphological studies using 1μm toluidine blue stained plastic sections revealed numerous spherical vacuoles within the perikarya and proximal dendrites of pyramidal neurons in the cerebral cortex and hippocampus of moribund YFP mice. The percentage of pyramidal neurons exhibiting cytoplasmic vacuoles in the cerebral cortex (60.8 ± 8.5%) exceeded the percentage of pyramidal neurons displaying dendritic beading in the same brain region (12.2 ± 2.7%). Similarly, the percentage of pyramidal neurons exhibiting cytoplasmic vacuoles in the hippocampus (21.7 ± 16.1%) exceeded the percentage of pyramidal neurons displaying dendritic beading in the hippocampus (0%). Vacuolation was also observed within the neuropil of the cerebral cortex and cerebellar white matter. Ultrastructurally, it was determined that these intracellular vacuoles corresponded to swollen mitochondria. Interestingly, some swollen mitochondria were localized in areas of swelling in neuronal processes and corresponded with the sites of beading.

Intracerebral models of rabies virus infection are characterized by widespread neuronal death (Jackson and Rossiter, 1997) and mitochondrial swelling, as well as swelling of the Golgi apparatus and extensive dilation of endoplasmic reticulum (Matsumoto, 1963; Jenson *et al.*, 1967; Fekadu *et al.,* 1988; Jackson and Rossiter 1997; Li *et al.*, 2005; Rasalingam *et al.*, 2005). Mitochondrial swelling is a typical indicator of lethal cellular injury (Trump *et al.*, 1974a). Neurons containing swollen mitochondria are labeled as 'moribund' because they are not yet dead, since in dead neurons mitochondria are collapsed (Emery *et al.*, 1987). Swelling of mitochondria is a common response of

neurons to glutamate (Olney, 1969; Olney, 1971; Randall and Thayer, 1992), epileptic activity (Olney *et al.*, 1983; Olney *et al.*, 1986) and cerebral ischemia (Garcia *et al.*, 1977; Kalimo *et al.*, 1977; Jenkins *et al.*, 1981), all of which are associated with excitotoxic neuronal injury. Mitochondrial swelling has also been observed in rabies virus infected cultures of mammalian neural tissues which displayed signs of neuronal degeneration (Matsumoto *et al.*, 1974). Peripheral inoculation, as previously mentioned, is characterized by inflammation of the brain and spinal cord, but not by prominent neuronal cell death (Reid and Jackson, 2001; Jackson, 2003). In this study, peripherally inoculated moribund YFP mice also showed minimal histopathological changes in paraffin embedded tissue sections and minimal staining for TUNEL or activated caspase-3. It is unclear if mitochondrial swelling following peripheral inoculation of rabies virus is caused by a similar underlying mechanism as that after intracerebral inoculation since neuronal degeneration is not a prominent feature of this model.

One mechanism of mitochondrial swelling involves elevated intracellular calcium (Bernardi *et al.*, 1998), which is also implicated in excitotoxic cell death. In cultured spinal cord neurons, exposure to NMDA or the calcium ionophore A23187 results in high amplitude mitochondrial swelling (Emery and Lucas, 1995). The resulting accumulation of intracellular calcium is believed to open the mitochondrial permeability transition pore (MTP), which allows the energy-independent diffusion of ions or low molecular weight sugars and metabolites into mitochondria, resulting in swelling (Bernardi *et al.*, 1998). However, in a previous study, we demonstrated that when rabies virus infected cultures of cortical and hippocampal neurons from mice were briefly exposed to glutamate, there was no increase in intracellular calcium (Weli *et al.*, 2006). Also, accumulation of intracellular calcium is associated with the degradation of microtubules and neurofilaments, which did

not occur to a significant degree in the present study (Emery et al., 1991). Thus, mitochondrial swelling in rabies virus infection, regardless of the route of inoculation, may not be due to excess intracellular calcium, particularly increases in calcium resulting from the activation of ionotropic glutamate receptors.

Mitochondrial swelling is also produced by the action of reactive oxygen species (ROS), which is a calcium independent mechanism (Galindo *et al.*, 2003). In rabies virus infection, elevations of inducible nitric oxide synthase (iNOS) mRNA, the product of which catalyzes the production of nitric oxide (NO), have been observed (Koprowski *et al.*, 1993). Direct measurements of NO using spin trapping also revealed a 30-fold increase in the CNS of CVS infected rats compared to controls (Hooper *et al.*, 1995). NO can go on to react with superoxide anion 0_2^- leading to the formation of peroxynitrate, which is a reactive oxygen species (Akaike *et al.*, 1995). However, superoxide-induced mitochondrial swelling is also associated with increases in caspase activity (Galindo *et al.*, 2003). In the present study, caspase-3 staining was rare in the cerebral cortex of moribund YFP mice and was absent in the hippocampus. Furthermore, oxidative stress is associated with the disruption of microtubules (Mirabelli *et al.*, 1989; Rogers *et al.*, 1989; Roediger and Armati, 2003), which was also not apparent in the present study.

Sodium and chloride may also play a role in mitochondrial swelling, as well as Golgi swelling (Emery *et al.,* 1991), both of which are observed in neurons following peripheral inoculation of YFP mice with CVS. Neurons injured in a low-calcium and low-chloride medium exhibit dilation of Golgi cisternae as well as an in increase in the electron opacity of mitochondria (Emery *et al.,* 1991). Monensin, a sodium ionophore, also causes dilation of Golgi cisternae. On the other hand, if chloride but not sodium is present in the medium, there is dilation of the mitochondria and cisternae of the smooth

endoplasmic reticulum. Dilated endoplasmic reticulum and high amplitude swelling of mitochondria are also observed in kidney slices incubated at 4°C, which disrupts the water balance and sodium pumps in these cells (Trump *et al.*, 1974b). As previously mentioned, sodium and chloride entry into neuronal processes are also implicated in the formation of varicosities (Lowe, 1978; Hasbani *et al.*, 1998). More specifically, sodium entry is believed to cause the intracellular movement of chloride to maintain electrical neutrality, which in turn draws water across the plasma membrane in order to maintain osmotic balance, thus resulting in varicosity formation (Al-Noori and Swann, 2000). This sequence of ionic movement also corresponds with the sequence of changes in organelle structure observed in this study. The initial entry of sodium agrees with our observation of some neurons which displayed swollen Golgi and morphologically normal mitochondria. The entry of chloride ions which follows sodium entry then results in mitochondrial swelling. This is typically followed by the swelling and fragmentation of endoplasmic reticulum, which results in the marked cytoplasmic vacuolation that is observed in severely degenerating neurons following mild hypothermia, NMDA application, exposure to the calcium ionophore A23187 (Emery and Lucas, 1995), dendritic transaction (Emery *et al.*, 1987; Emery *et al.*, 1991), intracerebral CVS inoculation in mice (Jenson *et al.*, 1967; Jackson and Rossiter, 1997) or rabies virus infection of cultured mammalian spinal and dorsal root ganglions (Matsumoto *et al.*, 1974). However, the intracellular vacuoles resulting from the fragmentation of endoplasmic reticulum are more numerous and irregularly shaped than the cytoplasmic vacuolation observed in the present study. This observation suggests that neurons in the peripheral model of rabies virus infection are not degenerating, or at least are not far along in the injury process, even when animals are moribund.

But do these swollen mitochondria result in the neuropil vacuolation observed in the cerebral cortex of moribund YFP mice? Charlton and colleagues (1984, 1987) observed what they described as spongiform lesions similar to those observed in the transmissible spongiform encephalopathies (TSE) in the cerebral cortex and thalamus of street rabies virus-infected skunks. They believed that these large space occupying lesions began as small membrane-bound vacuoles that were found predominantly in dendrites and rarely in axons, astrocytes or perikarya. The rapid enlargement of these vacuoles eventually resulted in the disruption of the vacuolar membrane and the surrounding plasma membrane, producing large spaces in the neuropil which often contained granular material and membrane fragments that originated from the initial disruption of the membrane-bound vacuoles and the plasma membrane of the affected cellular processes. However, it does not seem likely that the same process occurred in the present study. The membrane bound vacuoles in neurons of moribund YFP mice corresponded to mitochondria whereas the cytoplasm adjacent to the membrane-bound vacuoles usually contained normal organelles, including mitochondria, in the rabies virus infected skunks (Charlton *et al.*, 1987). Furthermore, these membrane-bound vacuoles observed by Charlton were rarely observed in the perikarya, but we observed vacuoles predominantly in the cell bodies of pyramidal neurons (60.8 ± 8.5%). Charlton (1984) also rarely observed rabies virions or matrix in neuronal processes containing vacuoles, while viral nucleocapsid was commonly observed next to swollen mitochondria in the present study. Lastly, the spongiform lesions described by Charlton and colleagues often contained granular material and membrane fragments, while the neuropil vacuolation in rabies virus infected mice often contained mitochondria and residual microtubule material. These observations suggest that the neuropil vacuolation observed in the present study

represented intracellular environments that are likely neuronal in origin. Furthermore, some of the vacuoles also contained synaptic vesicles or synaptic densities, which indicates that these vacuoles represented severely distended neuronal processes or swollen nerve endings. In some cases, however, the vacuoles were devoid of any residual material. As such, we cannot exclude the possibility that some of the neuropil vacuoles may represent swollen astrocytes, particularly those vacuoles surrounding blood vessels.

The structural changes observed in YFP mice challenge the hypothesis that neuronal dysfunction is responsible for the clinical features and fatal outcome in rabies virus infection. Typically, natural rabies and peripheral models of rabies virus infection are associated with relatively mild neuropathological changes and few degenerative neuronal changes. However, we observed changes not only in the morphology of neuronal processes, but also in organelle structure. These findings indicate that injury prominently involving neuronal processes may be sufficient to explain the severe clinical disease with a fatal outcome in rabies rather than neuronal dysfunction without morphological changes.

CHAPTER 8: SUMMARY AND CONCLUSIONS

We have examined the hypothesis that excitotoxicity may serve as a possible mechanism of neuronal dysfunction in rabies virus infection. However, the present study argues against a role for excitotoxicity in this fatal neurological infection. Ketamine, a non-competitive NMDA receptor antagonist, did not provide any beneficial effects clinically, histopathologically or by analysis of the number of infected neurons in ICR mice inoculated intracerebrally or peripherally with CVS. The morphological abnormalities in neuronal processes of moribund YFP mice inoculated peripherally with CVS also differed from the dendritic beading that is characteristic of excitotoxicity. We rarely observed structural changes in the dendrites of hippocampal pyramidal neurons, but did observe changes in the axons of pyramidal neurons in the cerebral cortex and axons in the cerebellum and brainstem. We also did not observe the microtubule fragmentation that is characteristically found in dendritic beads in excitotoxicity.

It is well established that animals inoculated peripherally with rabies virus do not exhibit prominent neuronal cytopathology or neuronal death (Reid and Jackson, 2001). However, in the present study, previously unrecognized changes in the morphology of neuronal processes and organelle structure were observed in moribund YFP mice. These structural changes may readily explain the severe clinical disease and fatal outcome in rabies virus infection. The focal constrictions between varicosities could cause electrical isolation of dendrites from neuronal perikarya. These findings support a role for severe neuronal injury without prominent neuronal death in rabies virus infection, as opposed to neuronal dysfunction without morphological changes.

Experiments should be undertaken to examine the role of sodium and chloride influx in mitochondrial swelling and beading of neuronal processes in rabies virus

infection. In particular, electrophysiological studies examining different sodium channels or the Na^+/K^+-pump could elucidate the mechanisms producing beading in neuronal processes. The electrophysiological properties of brain neurons infected by rabies virus have not yet been evaluated. Such studies would provide important information about the functional consequences of rabies virus infection.

REFERENCES

Adle-Biassette H, Bourhy H, Gisselbrecht M, Chretien F, Wingertsmann L, Baudrimont M, Portivel Y, Godeau B and F Gray (1996). Rabies encephalitis in a patient with AIDS: a clinicopathological study. *Acta Neuropathol* 92: 415-420.

Akaike T, Weihe E, Schaefer M, Fu ZF, Zheng YM, Vogel W, Schmidt H, Koprowski H and B Dietzschold (1995). Effect of neurotropic virus infection on neuronal and inducible nitric oxide synthase activity in rat brain. *J Neurovirol* 1: 118-125.

Al-Noori S and JW Swann (2000). A role for sodium and chloride in kainic acid-induced beading of inhibitory interneuron dendrites. *Neuroscience* 101: 337-348.

Babes V (1892). Sur certains caracteres des lesions histologiques de la rage. *Ann I Pasteur Paris* 6: 209-223.

Baer GM and TL Lentz (1991). Rabies pathogenesis to the central nervous system. In: Baer GM, editor. The natural history of rabies. Boca Raton: CRC Press; p105-120.

Bernardi P, Basso E, Colonna R, Castantini P, Di Lisa F, Eriksson O, Fontaine E, Forte M, Ochas F, Massari S, Nicolli A, Petronilli V and L Scorrano (1998). Perspectives on the mitochondrial permeability transition. *Biochimica et Biophysica Acta* 1365: 200-206.

Bouzamondo E, Ladogana A and H Tsiang (1993). Alteration of potassium-evoked 5-HT release from virus-infected rat cortical synaptosomes. *Neuroreport* 4: 555-558.

Bredesen DE (1995). Neural apoptosis. *Ann Neurol* 38: 839-851.

Bundza A and KM Charlton (1988). Comparison of spongiform lesions in experimental scrapie and rabies in skunks. *Acta Neuropathol* 76: 275-280.

Ceccaldi PE, Fillion MP, Ermine A, Tsiang H and G Fillion (1993). Rabies virus selectively alters 5-HT1 receptor subtypes in rat brain. *Eur J Pharmacol* 245: 129-138.

Ceccaldi PE, Gillet JP and H Tsiang (1989). Inhibition of the transport of rabies virus in the central nervous system. *J Neuropathol Exp Neurol* 48: 620-630.

Center for Disease Control and Prevention (1999). Human rabies prevention. *Morb Mortal Wkly Rep* 48: 1-21.

Chan WH, Sun WZ and TH Ueng (2005). Induction of rat hepatic cytochrome P-450 by ketamine and its toxicological implications. J Toxicol Env Heal A 68: 1581-1597.

Charlton KM (1984). Rabies: Spongiform lesions in the brain. *Acta Neuropathol (Berl)* 63: 198-202.

Charlton KM, Casey CA, Webster WA and A Bundza (1987). Experimental rabies in skunks and foxes: pathogenesis of the spongiform lesions. *Lab Invest* 57: 634-645.

Charlton KM and GA Casey (1979). Experimental rabies in skunks: immunofluorescence light and electron microscopic studies. *Lab Invest* 41: 36-44.

Charlton KM and GA Casey (1981). Experimental rabies in skunks: persistence of virus in denervated muscle at the inoculation site. *Can J Comp Med* 45: 357-362.

Charlton KM, Nadin-Davis S, Caset GA and AI Wandeler (1997). The long incubation period in rabies: delayed progression of infection in muscle at the site of exposure. *Acta Neuropathol* 94: 73-77.

Choi DW, Maulucci-Gedde MA and AR Kriegstein (1987). Pharmacology of glutamate neurotoxicity in cortical cell culture: attenuation by NMDA antagonists. *J Neurosci* 8: 185-196.

Collins RC and JW Olney (1982). Focal cortical seizures cause distant thalamic lesions. *Science* 218: 177.

Cornet E, Delpire E and R Gilles (1988). Relations between cell volume control, microfilaments and microtubules networks in T2 and PC12 cultured cells. *J Physiol* 83: 43-49.

Darman J, Backovic S, Dike S, Maragakis NJ, Krishnan C, Rothstein JD, Irani DN and DA Kerr (2004). Viral-induced spinal motor neuron death is non-cell-autonomous and involves glutamate excitotoxicity. *J Neurosci* 24: 7566-7575.

Daugas E, Nochy D, Ravagnan L, Loeffler M, Susin SA, Zamzami N and G Kroemer. (2000). Apoptosis-inducing factor (AIF): a ubiquitous mitochondrial oxidoreductase involved in apoptosis. *FEBS Lett* 476: 118-123.

Dhingra V, Li X, Liu Y and ZF Fu (2007). Proteomic profiling reveals that rabies virus infection results in differential expression of host proteins involve in ion homeostasis and synaptic physiology in the central nervous system. *J Neurovirol* 13:107-117.

Dumrongphol H, Srikiatkhoachorn A, Hemachudha T, Hotchabhakdi B and P Govitrapong (1996). Alteration of muscarinic acetylcholine receptors in rabies viral-infected dog brains. *J Neurol Sci* 137: 1-6.

Emery DG and JH Lucas (1995). Ultrastructural damage and neuritic beading in cold-stressed spinal neurons with comparisons to NMDA and A23187 toxicity. *Brain Res* 692: 161-173.

Emery DG, Lucas JH and GW Gross (1987). The sequence of ultrastructural changes in cultured neurons after dendritic transaction. *Exp Brain Res* 67: 41-51.

Emery DG, Lucas JH and GW Gross (1991). Contributions of sodium and chloride to ultrastructural damage after dendrotomy. *Exp Brain Res* 86: 60-72.

Fan T, Han L, Cong R and J Liang (2005). Caspase family proteases and apoptosis. *Acta Biochemica Biophysica Sinica* 37: 719-727.

Fekadu M, Shaddock JH, Chandler FW and DW Sanderlin (1988). Pathogenesis of rabies virus from a Danish bat (*Eptesicus serotinus*): neuronal changes suggestive of spongiosis. *Arch Virol* 99: 187-203.

Feng G, Mellor RH, Bernstein M, Keller-Peck C, Nguyen QT, Wallace M, Nerbonne JM, Lichtman JW and JR Sanes (2000). Imaging neuronal subsets in transgenic mice expressing multiple spectral variants of GFP. *Neuron* 28: 24-51.

Fu ZF and AC Jackson (2005). Neuronal dysfunction and death in rabies virus infection. *J Neurovirol* 11: 101-106.

Fu ZF, Weihe E, Zheng YM, Schafer MK, Sheng H, Corisdeo S, Rauscher FJ, Koprowski H and B Dietzschold (1993). Differential effects of rabies and borna disease viruses on immediate-early- and late-response gene expression in brain tissues. *J Virol* 67: 6674-6681.

Galindo MF, Jordan J, Gonzales-Garcia C and V Cena (2003). Reactive oxygen species induce swelling and cytochrome c release but not transmembrane depolarization in isolated rat brain mitochondria. *Brit J Pharmacol* 139: 797-804.

Garcia JH, Kalimo H, Kaminjyo Y and BF Trump (1977). Cellular events during partial ischemia. I. Electron microscopy of feline cerebral cortex after middle-cerebral-artery occlusion. *Virchows Arch B Cell Pathol* 25: 191-206.

Gaudin Y, Tuffereau C, Durrer P, Brunner J, Flamand A and R Ruigrok (1999). Rabies virus-induced membrane fusion. *Mol Membr Biol* 16: 21-31.

Gill R and D Lodge (1997). Pharmacology of AMPA antagonists and their role in neuroprotection. *Int Rev Neurobiol* 40: 197-232.

Gonzalez-Angulo A, Marquez-Monter H, Feria-Velasco A and BJ Zavala (1970). The ultrastructure of Negri bodies in Purkinje neurons in human rabies. *Neurology* 10: 323-328.

Gosztonyi G, Dietzschold B, Kao M, Rupprecht CE, Ludwig H and H Koprowski (1993). Rabies and Borna disease. A comparative pathogenetic study of two neurovirulent agents. *Lab Invest* 68: 285-295.

Gosztonyi G and H Ludwig (2001). Interactions of viral proteins with neurotransmitter receptors may protect or destroy neurons. *Curr Top Microbiol Immunol* 253: 121-144.

Gourmelon P, Briet D, Clarencon D, Court L and H Tsiang (1991). Sleep alterations in experimental street rabies virus infection occur in the absence of major EEG abnormalities. *Brain Res* 554: 19-165.

Gourmelon P, Briet D, Court L and H Tsiang (1986). Electrophysiological and sleep alterations in experimental mouse rabies. *Brain Res* 398: 128-140.

Guigoni C and P Coulon (2002). Rabies virus is not cytolytic for rat spinal motorneurons *in vitro*. *J Neurovirol* 8: 306-317.

Guler G, Erdogan F, Golgeli A, Akin A and A Boyaci (2005). Ketamine reduces lidocaine-induced seizures in mice. *Int J Neurosci* 115: 1239-1244.

Hasbani MJ, Hyrc KL, Faddis BT, Romano C and MP Goldberg (1998). Distinct roles for sodium, chloride and calcium in excitotoxic dendritic injury and recovery. *Exp Neurol* 154: 241-258.

Hellenbrand W, Meyer C, Rasch G, Steffens I and A Ammon (2005). Cases or rabies in Germany following organ transplantation. *Eurosurveillance Weekly* 10.

Hemachudha T, Sunsaneewitayakul B, Desudchit T, Suankratay C, Sittipunt C, Wacharapluesadee S, Khawplod P, Wilde H and AC Jackson (2006). Failure of therapeutic coma and ketamine for therapy of human rabies. *J Neurovirol.* 12: 407-409.

Hooper DC Ohnishi ST, Kean R, Numagami Y, Dietxschold B and H Koprowski (1995). Local nitric oxide production in viral and autoimmune diseases of the central nervous system. *Proc Natl Acad Sci USA* 92: 5312-5316.

Hoskison MM and CW Shuttleworth (2006). Microtubule disruption, not calpain-dependent loss of MAP2, contributes to enduring NMDA-induced dendritic dysfunction in acute hippocampal slices. *Exper Neurol* 202: 301-312.

Hoskison MM, Yanagawa Y, Obata K and CW Shuttleworth (2007). Calcium-dependent NMDA-induced dendritic injury and MAP2 loss in acute hippocampal slices. *Neurosci* 145: 66-79.

Ikegaya Y, Kim J, Baba M, Iwatsuo T, Nishiyama N and N Matsuki (2001). Rapid and reversible changes in dendrite morphology and synaptic efficacy following NMDA receptor activation: implication for a cellular defense against excitotoxicity. *J Cell Sci* 114: 4083-4093.

Iwasaki Y, Sako K, Tsunoda I and Y Ohara (1993). Phenotypes of mononuclear cell infiltrates in human central nervous system. *Acta Neurophatol* 85: 653-657.

Iwata M, Komori S, Unno T, Mnamoto N and H Ohashi (1999). Modification of membrane currents in mouse neuroblastoma cells following infection with rabies virus. *Br J Pharmacol* 126: 1691-1698.

Jackson AC (1993). Cholinergic system in experimental rabies in mice. *Acta Virol* 37: 502-508.

Jackson AC (2000). Rabies. *Can J Neurol Sci* 27: 278-282.

Jackson AC (2003). Neuronal apoptosis in experimental rabies: role of the route of viral entry. *Neurology* 60(Suppl 1): A102.

Jackson AC (2006). Rabies: new insights into pathogenesis and treatment. *Curr Opin Neurol* 19: 267-270.

Jackson AC (2007). Pathogenesis. In: Jackson AC, Wunner WH, eds. Rabies, Second Edition, pp 341-381. London: Elsevier Academic Press.

Jackson AC and DL Reimer (1989). Pathogenesis of experimental rabies in mice: an immunohistochemical study. *Acta Neuropathol* 78: 159-165.

Jackson AC and H Park (1998). Apoptotic cell death in experimental rabies in suckling mice. *Acta Neuropathol* 95: 159-164.

Jackson AC and JP Rossiter (1997). Apoptosis plays an important role in experimental rabies virus infection. *J Virol* 71: 5603-5607.

Jackson AC, Rasalingam P and SC Weli (2006). Comparative pathogenesis of recombinant rabies vaccine strain SAD-L16 and SAD-D29 with replacement of Arg333 in the glycoprotein after peripheral inoculation of neonatal mice: less neurovirulent strain is a stronger inducer of neuronal apoptosis. *Acta Neuropathol* 111: 372-378.

Jackson AC, Scott CA, Owen J, Weli SC and JP Rossiter (2007). Therapy with minocycline aggravates experimental rabies in mice. *J Virol* 81: 6248-6253.

Jackson AC, Ye H, Phelan CC, Ridaura-Sanz C, Zheng Q, Li Z, Wan X and E Lopez-Corella (1999). Extraneural organ involvement in human rabies. *Lab Invest* 79: 945-951.

Jacob Y, Badrane H, Ceccaldi PE and N Tordo (2000). Cytoplasmic dynein LC8 interacts with lyssavirus phosphoprotein. *J Virol* 74: 10217-10222.

Jenkins JW, Povlishock JT, Lewelt W, Miller D, and DP Becker (1981). The role of postischemic recirculation in the development of neuronal injury following complete cerebral ischemia. *Acta Neuropathol* 55: 205-220.

Jenson AB, Rabin ER, Wende RD and JL Melnick (1967). A comparative light and electron microscopic study of rabies and hart park virus encephalitis. *Exp Mol Pathol* 7: 1-10.

Juntrakul S, Ruangvejvorachai P, Shuangshoti S, Wacharapluesadee S and T Hemachudha (2005). Mechanisms of escape phenomenon of spinal cord and brainstem in human rabies. *BMC Infect Dis* 5: 104-112.

Kalimo H, Garcia JH, Kamijyo, Tanaka J and BF Trump (1977). The ultrastructure of "brain death." II. Electron microscopy of feline cortex after complete ischemia. *Virchows Arch B Cell Pathol* 25: 207-220.

Kelly RM and PL Strick (2000). Rabies as a transneuronal tracer of circuits in the central nervous system. *J Neurosci Methods* 103: 63-71.

Koh J, Goldberg MP, Hartley DM and DW Choi (1990). Non-NMDA receptor-mediated neurotoxicity in cortical culture. *J Neurosci* 10: 693-705.

Koprowski H, Zheng YM, Heber-Katz E, Fraser N, Rorke L, Fu ZF, Hanlon C and B Dietschold (1993). In vivo expression of inducible nitric oxide synthase in experimentally induced neurologic disease. *Proc Natl Acad Sci USA* 90: 3024-3027.

Kristensson K, Dastur DK, Manghani DK, Tsiang H and M Bentivoglio (1996). Rabies: interactions between neurons and viruses: a review of the history of Negri inclusion bodies. *Neuropath App Neuro* 22: 179-187.

Langevin C, Jaaro H, Bressanelli S, Fainzilber M and C Tuffereau (2002). Rabies virus glycoprotein (RVG) is a trimeric ligand for the N-terminal cysteine-rich domain of the mammalian p75 neurotrophin receptor. *J Biol Chem* 277: 37655-62.

Lee JM, Zipfel GJ and DW Choi (1999). The changing landscape of ischaemic brain injury mechanisms. *Nature* 399: A7-A14.

Leist M and M Jaattela (2001). Four deaths and a funeral: from caspases to alternative mechanisms. *Nat Rev Mol Cell Biol* 2: 589-598.

Lentz TL, Burrage TG, Smith AL, Crick J and GH Tignor (1982). Is the acetylcholine receptor a rabies virus receptor? *Science* 215: 182-184.

Lewis P, Fu Y and TL Lentz (2000). Rabies virus entry at the neuromuscular junction in nerve-muscle cocultures. *Muscle Nerve* 23: 720-730.

Li X-Q, Sarmento L and ZF Fu (2005). Degeneration of neuronal processes after infection with pathogenic, but not attenuated, rabies virus. *J Virol* 79: 10063-10068.

Lockhart BP, Tordo N and H Tsiang (1992). Inhibition of rabies virus transcription in rat cortical neurons with the dissociative anaesthetic ketamine. *Antimicrob Agents Ch* 36: 1750-1755.

Lockhart BP, Tsiang H, Ceccaldi PE and S Guillemer (1991). Ketamine-mediated inhibition of rabies virus infection *in vitro* and in rat brain. *Antivir Chem Chemo* 2: 9-15.

Love S and CA Wiley (2002). Viral diseases. In: *Greenfield's Neuropathology* (D. I. Graham and P. L. Lantos, eds). Pg1-105. London: Arnold.

Lowe DA (1978). Morphological changes in the cat cerebral cortex produced by superfusion of ouabain. *Brain Res* 148: 347-363.

Matsumoto S (1963). Electron microscope studies of rabies virus in mouse brain. *J Cell Biol* 19: 565-591.

Matsumoto S, Schneider G, Kawai A and T Yonesawa (1974). Further studies on the replication of rabies and rabies-like viruses in organized cultures of mammalian neural tissues. *J Virol* 14: 981-996.

Mirabelli F, Salis A, Vairetti M, Bellomo G, Thor H and S Orrenius (1989). Cytoskeletal alterations in human platelets exposed to oxidative stress are mediated by oxidative and Ca2+-dependent mechanisms. *Arch Biochem Biophys* 270: 478-488.

Miyamoto K and S Matsumoto (1967). Comparative studies between pathogenesis of street and fixed rabies infection. *J Exp Med* 125: 447-456.

Morimoto K, Hooper DC, Spitsin S, Koprowski H and B Dietzschold (1999). Pathogenicity of different rabies virus variants inversely correlates with apoptosis and rabies virus glycoprotein expression in infected primary neuron cultures. *J Virol* 73: 510-518.

Moscoso LM, Cremer H and JR Sanes (1998). Organization and reorganization of neuromuscular junctions in mice lacking neural cell adhesion molecule, tenascin-C, or fibroblast growth factor-5. *J Neurosci* 18: 1465-1477.

Nadler JV, Perry BW and CW Cotman (1977). Selectivity in the destruction of hippocampal neurons by kainic acid. *Neurosci Abstr* 3: 202.

Nakajima T, Wang RS, Elovaara E, Park SS, Gelboin HV and H Vainio (1993). Cytochrome P-450-related difference between rats and mice in the metabolism of benzene, toluene and trichloroethylene in liver microsomes. *Biochem Pharmacol* 45: 1079-1085.

Nargi-Aizenman JL and DE Griffin (2001). Sindbis virus-induced neuronal death is both necrotic and apoptotic and is ameliorated by N-methyl-D-aspartate receptor antagonists. *J Virol* 75: 7114-7121.

Nath A, Haughey NJ, Jones M, Anderson C, Bell JE and JD Geiger (2000). Synergistic neurotoxicity by human immunodeficiency virus proteins Tat and gp120: protection by memantine. *Ann Neurol* 47: 186-194.

Negri A (1903). Beitrag zum Studium der Aetiologie der Tollwuth. *Z Hyg Infektionskr* 43: 507-528.

Negri A (1909). Uber die Morphologie und der Entwicklungszyklus des Parasiten der Tollwut (Neurocytes hydrophobiae Calkins). *Z Hyg Infektionskr* 63: 421-440.

Nicotera P and S Orrenius (1998). The role of calcium in apoptosis. *Cell Calcium* 23: 173-180.

Oldstone MBA (1984). Virus can alter cell function without causing cell pathology: disordered function leads to imbalance in homeostasis and disease. In: Notkins AL, Oldsteon MBA (eds) Concepts in viral pathogenesis. Springer Verlag, New York, Heidelberg, Tokyo.

Olney JW (1969). Glutamate-induced retinal degeneration in neonatal mice. Electron microscopy of the acutely evolving lesion. *J Neuropathol Exp Neurol* 28: 455-474.

Olney JW (1971). Glutamate-induced neuronal necrosis in the infant mouse hypothalamus. *J Neuropathol Exp Neurol* 30: 75-90.

Olney JW, Collins RC and RS Sloviter (1986). Excitatory mechanisms of epileptic brain damage. *Adv Neurol* 44: 857-877.

Olney JW, deGubareff T and RS Sloviter (1983). 'Epileptic' brain damage in rats induced by sustained electrical stimulation of perforant path. II. Ultrastructural analysis of acute hippocampal pathology. *Brain Res Bull* 10: 699-712.

Olney JW, Fuller T and T de Gubareff (1979). Acute dendrotoxic changes in the hippocampus of kainate treated rats. *Brain Res* 176: 91.

Oliva AA, Lam TT and JW Swann (2002). Distally directed dendrotoxicity induced by kainic acid in hippocampal interneurons of green fluorescent protein-expressing transgenic mice. *J Neurosci* 22: 8052-8062.

Olson ME and P Renchko (1988). Azaperone and azaperone-ketamine as a neuroleptic sedative and anesthetic in rats and mice. *Lab Anim Sci* 38: 299.304.

Park JS, Bateman MC and MP Goldberg (1996). Rapid alterations in dendrite morphology during sublethal hypoxia or glutamate receptor activation. *Neurobiol Dis* 3: 215-227.

Polo-Parada L, Bose CM and LT Landmesser (2001). Alterations in transmission, vesicle dynamics, and transmitter release machinery at NCAM-deficient neuromuscular junctions. *Neuron* 32: 815-828.

Prosniak M, Hooper DC, Dietzschold B and H Koprowski (2001). Effect of rabies virus infection n gene expression in mouse brain. *PNAS* 90: 2758-2763.

Purpura DP, Bodick N, Suzuki M, Rapin I and S Wurzelmann (1982). Microtubule disarray in cortical dendrites and neurobehavioural failure. I. Golgi and electron microscopic studies. *Devl Brain Res* 5: 287-297.

Randall RD and SA Thayer (1992). Glutamate-induced calcium transient triggers delayed calcium overload and neurotoxicity in rat hippocampal neurons. *J Neurosci* 12: 1882-1895.

Rasalingam P, Rossiter JP and AC Jackson (2005). Recombinant rabies virus vaccine strain SAD-L16 inoculated intracerebrally in young mice produces severe encephalitis with extensive neuronal apoptosis. *Can J Vet Res* 69: 100-105.

Raux H, Flamand A and D Blondel (2000). Interaction of the rabies virus P protein with the LC8 dynein light chain. *J Virol* 74: 10212-10216.

Razvi ES and RM Welsh (1995). Apoptosis in viral infections. *Adv Virus Res* 45: 1-60.

Reagan KJ and WH Wunner (1985). Rabies virus interaction with various cell lines is independent of the acetylcholine receptor. *Arch Virol* 84: 277-282.

Reed JC (1998). Bcl-2 family proteins. *Oncogene* 17: 3225-3236.

Reid JE and AC Jackson (2001). Experimental rabies virus infection in Artibeus jamaicensis bats with CVS-24 variants. *J Neurovirol* 7: 511-517.

Rodriguez CI and SM Dymecki (2000). Origin of the precerebellar system. *Neuron* 27: 475-486.

Roediger B and PJ Armati (2003). Oxidative stress induces axonal beading in cultured human brain tissue. *Neurobiol Dis* 13: 222-229.

Rogers KR, Morris CD, and DR Blake (1989). Cytoskeletal rearrangement by oxidative stress. *Int J Tissue React* 11: 309-314.

Rossiter JP and AC Jackson (2007). Pathology. In: Jackson AC, Wunner WH, eds. Rabies, Second Edition. London: Elsevier Academic Press.

Sakai T, Ichiyama T, Whiteen CW, Giesecke AH and JM Lipton (2000). Ketamine suppresses endotoxin-induced NF-κB expression. *Can J Anesth* 47: 1019-1024.

Shankar V, Dietzschold B and H Koprowski (1991). Direct entry of rabies virus into the central nervous system without prior local replication. *J Virol* 65: 2736-2738.

Springer JE, Azbill RD, Kennedy SE, Genrge J and JW Geddes (1997). Rapid calpain I activation and cytoskeletal protein degradation following traumatic spinal cord injury: attenuation with riluzole pretreatment. *J Neurochem* 69: 1592-1600.

Srinivasan A, Kuehnert MJ, Ksiazek TG, Shieh WJ, Guarner J, Zaki SR, Paddock CD, Hanlon CA, Likos A, Jernigan DB, Goldsmith C, Cardo D, Niezgoda M, Rupprecht C, LeDuc J, Burton EC, Sutker WL, Zoretic J, Fischbach B, El-Feky WH, Orciari L, Sanchez EQ, Klintmalm GB and ME Chamberland (2005). Transmission of rabies virus from an organ donor to four transplant recipients. *N Engl J Med* 352: 1103-1111.

Susin SA, Zamzami N, Castedo M, Hirsch T, Marchetti P, Macho A, Daugas E, Geuskens M and G Kroemer (1996). Bcl-2 inhibits the mitochondrial release of an apoptogenic protease. *J Exp Med* 184: 1331-1341.

Tang Y, Rampin O, Giuliano F and G Ugolini (1999). Spinal and brain circuits to motorneurons of the bulbospongiosus muscle: retrograde transneuronal tracing with rabies virus. *J Comp Neurol* 414: 167-192.

Tangchai P, Yanbutr D and A Vejjajiva (1970). Central nervous system lesions in human rabies: a study of twenty-four cases. *J Med Assoc Thailand* 53: 471-488.

Theerasurakarn S and S Ubol (1998). Apoptosis induction in brain during the fixed strain of rabies virus infection correlates with onset and severity of illness. *J Neurovirol* 4: 407-414.

Thompson CB. Apoptosis in the pathogenesis and treatment of disease. *Science* 267: 1456-1462.

Thoulouze MI, Lafage M, Schachner M, Hartmann U, Cremer H and M Lafon (1998). The neural cell adhesion molecule is a receptor for rabies virus. *J Virol* 72:7181-7190.

Thoulouze MI, Lafage M, Yuste VJ, Baloul L, Edelman L, Kroemer G, Israel N, Susin SA and M Lafon (2003). High level of Bcl-2 counteracts apoptosis mediated by a live rabies virus vaccine strain and induces long-term infection. *Virology* 314: 549-561.

Trump BF, Laiho KA, Mergner WJ and AU Arstile (1974a). Studies on the subcellular pathophysiology of acute lethal cell injury. *Beit Path* 152: 243-271.

Trump BF, Strum JM and AE Bulger (1974b). Studies on the pathogenesis of ischemic cell injury. I. Relation between ions and water shifts and ultrastructure in rat kidney slices during swelling at 0-4°C. *Virchows Arch B Cell Pathol* 16: 1-34.

Tsiang H (1979). Evidence for an intraaxonal transport of fixed and street rabies virus. *J Neuropathol Exp Neurol* 38: 286-296.

Tsiang H (1982). Neuronal function impairment in rabies-infected rat brain. *J Gen Virol* 61: 277-281.

Tsiang H, Ceccaldi PE and E Lycke (1991a). Rabies virus infection and transport in human sensory dorsal root ganglia neurons. *J Gen Virol* 72: 1191-1194.

Tsiang H, Ceccaldi PE, Ermine A, Lockhart B and S Guillemer (1991b). Inhibition of rabies virus infection in cultured rat cortical neurons by N-methyl-D-aspartate noncompetitive antagonist, MK-801. *Antimirob Agents Ch* 35: 572-574.

Tuffereau C, Benejean J, Blondel D, Kieffer B and A Flamand (1998). Low-affinity nerve-growth factor receptor (P75NTR) can serve as a receptor for rabies virus. *EMBO J* 17: 7250-7259.

Ubol S, Sukwattanapan C and Maneerat Y (2001). Inducible nitric oxide synthase inhibition delays death of rabies virus-infected mice. *J Med Microbiol* 50: 238-242.

Van Dam A-M, Bauer J, Man-A-Hing WK, Marquette C, Tiders FJ and F Berkenbosch (1995). Appearance of inducible nitric oxide synthase in the rat central nervous system after rabies virus infection and during experimental allergic encephalomyelitis but not after peripheral administration of endotoxin. *J Neurosci Res* 40: 251-260.

Vanicky I, Marsala M and TL Yaksh (1998). Neurodegeneration induced by reversed microdialysis of NMDA; a quantitative model for excitotoxicity in vivo. *Brain Res* 789: 347-350.

Warrell MJ and DA Warrell (2004). Rabies and other lyssavirus diseases. *Lancet* 363: 959-969.

Weiss J and S Sensi (2000). Ca^{2+} - Zn^{2+} permeable AMPA or kainite receptors: possible key factors in selective neurodegeneration. *Trends Neurosci* 23: 365-371.

Weli SC, Scott CA, Ward CA and AC Jackson (2006). Rabies virus infection of primary neuronal cultures and adult mice: failure to demonstrate evidence of excitotoxicity. *J Virol* 80: 10270-10273.

Willoughby RE Jr, Rieves KS, Hoffman GM, Ghanayem S, Amlie-Lefond CM, Schwabe MJ, Chusid MH and CE Rupprecht (2005). Survival after treatment of rabies with induction of coma. *N Engl J Med* 352: 2508-2514.

World Health Organization (2005). WHO expert consultation on rabies: first report. Geneva: World Health Organization.

Wunner WH (2007). Rabies virus. In: Jackson AC, Wunner WH, eds. Rabies, Second Edition, pp 23-68. London: Elsevier Academic Press.

Xue D, Huang Z, Barnes K, Lesiuk HJ, Smith KE and AM Buchan (1994). Delayed treatment with AMPA, but not NMDA, antagonists reduces neocortical infarction. *J Cereb Blow Flow Metab* 13: 251-261.

Yang J, Liu C, Bhalla K, Kim CN, Ibrado AM, Cai J, Peng TI, Jones DP and X Wang (1997). Prevention of apoptosis by Bcl-2: release of cytochrome c from the mitochondria blocked. *Science* 275: 1129-1132.

Yatim N, Billig I, Compoint C, Buisseret P and C Buisseret-Delmas (1996). Trigeminocerebellar and trigemino-olivary projections in rats. *Neurosci Res* 25: 267-283.